Check for updates

Advancements in Controlled Source Electromagnetic Methods for Prospecting Unconventional Hydrocarbon Resources in China

Liangjun Yan[1,2,3]

Abstract

Globally, unconventional hydrocarbons, known for the symbiosis of their hydrocarbon source and reservoir, pose significant seismic exploration challenges due to their confined target regions, extensive burial depth, minimal acoustic impedance variation, marked heterogeneity, and strong anisotropy. Over the past decade, electromagnetic (EM) exploration has evolved markedly, improving resolution and reliability, thus becoming indispensable in unconventional hydrocarbon exploration. Focusing on China's application of the controlled source electromagnetic method (CSEM), this review examines the geological and electrical attributes of these reservoirs, notably the low resistivity, high polarization and strong electrical anisotropy of shale gas reservoirs. Despite the demonstrated positive correlation between induced polarization (IP) parameters and reservoir parameters, current methodologies emphasize the IP effect, inadvertently neglecting electrical anisotropy, which affects data precision. Moreover, single-source CSEM methodologies limit the observational components, acquisition density, and exploration area, impacting the accuracy and efficacy of data interpretation. Recently developed CSEM techniques in China, namely wide-frequency electromagnetic method (WFEM), time–frequency electromagnetic method (TFEM), long offset transient electromagnetic method (LOTEM), and wireless electromagnetic method (WEM), harness high-power pseudo-random binary sequence (PRBS) waveforms, reference observation and processing technology, hybrid inversion, and enhancing operational efficiency and adaptability despite the pressing need for multi-functional software for data acquisition. Case studies detail these methods' applications in shale gas sweet spot detection and continuous hydraulic fracturing monitoring, highlighting the immense potential of EM methods in unconventional hydrocarbon sweet spot detection and total organic content (TOC) predication. However, challenges persist in suppressing EM noise, streamlining 3D inversion processes, and improving the detection and evaluation of sweet spots.

Keywords CSEM · Resistivity · Induced polarization · Polarizability · Unconventional hydrocarbon resources · TOC · Sweet spot · Hydraulic fracturing monitoring

---

Extended author information available on the last page of the article

Article Highlights

- A comprehensive shale gas sweet spot model and parameter prediction method have been constructed, providing a robust physical foundation for shale gas exploration and sweet spot detection via the Controlled Source Electromagnetic Method (CSEM) method
- Significant enhancements in the resolution and dependability of four other methods have been made through the implementation of various key technologies
- Case studies confirm that CSEM has the capacity to facilitate shale gas exploration, sweet spot detection, and the monitoring of hydraulic fracturing operations to yield satisfactory geological outcomes

1 Introduction

Currently, the trajectory of oil and gas exploration is trending toward the investigation of deep and ultra-deep reservoirs (> 5000 m), extending the exploration domain from conventional to unconventional oil and gas. Paramount issues in the exploration and development of unconventional hydrocarbon (HC) reservoirs now comprise fluid identification, sweet spot (the area where unconventional HC is rich, easy to develop, and economically beneficial, in terms of oil and gas contents, porosity, brittleness, TOC and permeability) detection, and the optimization of enhanced oil recovery (EOR). Despite the seismic exploration method's fundamental role in sweet spot detection and development, largely due to its high resolution and attribute identification capability, there are unique challenges in certain locales. For instance, most shale gas exploration areas in Southern China feature rugged terrains covered by limestone, rendering seismic exploration significantly costlier and complicating the acquisition of high-quality data. Further complicating matters, sweet spots typically inhabit argillaceous source rocks characterized by deep burial depth, organic matter richness, exceptionally low porosity and permeability, and pronounced heterogeneity. Their acoustic wave impedance shows minimal deviation from the surrounding rocks and traps are absent, thereby exacerbating detection difficulties and reservoir parameter prediction. Thus, the development of high-precision seismic prediction methods for HC reservoirs poses significant challenges. Existing research indicates that electrical property parameters—resistivity, polarizability, and anisotropy—are more sensitive to reservoir fluids than seismic parameters, thereby offering an advantage to the EM method for unconventional HC exploration and development (Vinegar and Waxman1984; Xiang et al. 2014; Burtman et al. 2014; Burtman and Zhdanov 2015; Adao et al. 2016; Wang et al. 2022). Rapid advancements in electromagnetic (EM) instrumentation and data acquisition technology, along with the evolution of EM exploration methodologies (He et al. 2010; Strack 2013; Tietze et al. 2014; He 2019), have made the application to unconventional oil and gas exploration and development feasible (Zhang et al. 2013; Passalacqua and Strack 2016). Over the past decade, numerous researchers and industry professionals have undertaken studies on the electrical characteristics of unconventional oil and gas reservoirs, founded on unconventional oil and gas geological theory. This has led to the establishment of unconventional reservoir geoelectric models and reservoir parameter prediction models based on electrical properties, in turn forming fluid identification, sweet spot detection, and evaluation methods for unconventional oil and gas. These developments have solidified the petrophysical basis for the effective application of EM methods (Yan et al. 2014; Chen et al. 2021).

Concurrent with this, efforts to research and develop new methods and technologies for EM exploration have been bolstered. It is well-established that CSEM methods constitute a pivotal subcategory within the sphere of electromagnetic geophysical exploration. Among these, the terrestrial long-conductor sourced electromagnetic technique emerges as particularly noteworthy, endowed with a suite of salient attributes encompassing substantial exploration depths, acute sensitivity to high-impedance anisotropic strata, gradual attenuation of the invoked electromagnetic field, extensive survey range, and augmented operational efficacy (Strack et al. 1989; Strack 1992, 2013). These attributes render it instrumental in hydrocarbon exploration. In an evolutionary trajectory, advancements have been observed in China concerning the fundamental theory of CSEM, inclusive of forward and inverse modeling, acquisition technology, and instrumentation. Addressing the limitations of Controlled Source Audio-frequency Magnetotellurics (CSAMT) in far-zone operation, such as attenuated signals and decreased efficiency, He and Wang (2007), He (2010) introduced the WFEM technique. This approach is predicated on the utilization of pseudo-random signaling for the electromagnetic source, while concurrently observing multifarious frequency domains of the electromagnetic field, thereby bolstering both efficacy and resilience to interference. Notably, He and Wang (2007) amalgamated the merits of CSEM and LOTEM, and extrapolating from the Russian high-power field establishment modality, postulated the TFEM. This innovative approach encompasses simultaneous acquisition of time-domain and frequency-domain electromagnetic field components, followed by domain-specific processing. Additionally, it incorporates definitions of apparent resistivity, apparent polarization rate, and phase parameters pertinent to reservoir characterization. Utilizing the polarization patterns induced in hydrocarbon reservoirs, this methodology enhances fluid identification and 'sweet spot' detection.

Moreover, Di et al. (2008) presented an intriguing proposition with the WEM technique based on "skywave" observation. Predicated on the full-space "Ionosphere-Strata" model, wherein the electromagnetic fields incited by a grounded extended conductor source propagate in a waveguide fashion exhibiting attenuated decay and protracted transmission, the method synergizes the attributes of magnetotellurics (MT) and CSAMT. Employing a horizontal line source that is commensurate with the ionospheric thickness, this method transmits a spectrum of frequencies in the 0.1–300 Hz range, considerably extending the far-zone range and empowering resource exploration within mainland China.

Collectively, these burgeoning methodologies are characterized by the adoption of cutting-edge techniques such as defining electromagnetic attributes, deploying high-power pseudo-random current waveforms, skywave observation, near-reference observation, and comprehensive inversion constrained by well-seismic data. These developments, epitomizing a paradigm shift, have not only augmented fluid identification and sweet spot detection capacities within the domain of unconventional hydrocarbon exploration but have also markedly bolstered the reliability, efficacy, and resolution of the techniques, thereby furnishing technical and methodological assurances for the exploration and development of unconventional oil and gas reserves.

Numerous reviews have synthesized the application of EM methods and technologies within conventional hydrocarbon (HC) exploration and development. These techniques enhance resolution via innovation in data acquisition, processing, and inversion methodologies, deploying the distinct attributes of high resistance and strong anisotropy for hydrocarbon reservoir identification (Strack et al. 1989; ConsTable 2010; He et al. 2010; Strack 2013; Tietze et al. 2014; Streich 2016; Di et al. 2019, 2020; He 2019; Xue et al. 2020a, b; Liu et al. 2021).

This review concentrates on the examination of the electrical characteristics of unconventional reservoirs, the detection of sweet spots, and associated characteristic parameters prediction methodologies predicated on the IP model. We also cover the advances made concerning novel methods and technologies within EM exploration. Furthermore, we present several case studies demonstrating the application of the CSEM method for shale gas sweet spot detection and hydraulic fracturing monitoring.

1.1 Geological and Electrical Characteristics of Unconventional HC Reservoirs

Unconventional hydrocarbon (HC) reservoirs exhibit several geologic features, as delineated by Zou et al. (2015a, b): (a) source–reservoir symbiosis (i.e., the mutual existence of source rock and reservoir); (b) extensive distribution, considerable depth of burial, and blurred boundaries; (c) compact structure, unfavorable physical properties, reduced porosity and permeability, abundant nanofractures, and significant heterogeneity; (d) a wide variety of lithological constituents, including sandstone, limestone, shale, coal, and migmatite; and (e) a high content of organic matter, advanced maturity, inefficient phase separation, and the lack of a clear divide between oil, gas, and water. Inevitably, these geological attributes of unconventional reservoirs lead to distinctive physical characteristics. In general, unconventional reservoirs display low porosity, permeability, magnetic susceptibility, velocity, and density, but they demonstrate high resistivity. These electrical traits of shale reservoirs are particularly distinct (Zonge and Wynn 1975; Seigel et al. 2007; Davydycheva et al. 2006; Wang et al. 2015; Burtman and Zhdanov 2015; Hu et al. 2022). To exemplify the importance of electrical anisotropy, Strack (2013) presented a model of sand/shale sequences commonly found in many basins. This model exhibits thin laminations throughout, resulting in electrical anisotropy. Typical anisotropy values (vertical resistivity/horizontal resistivity) range between 1.2 and 1.4 in sedimentary basins, but can increase up to 10. Standard induction logs and MT soundings provide only horizontal resistivities, heavily influenced by shales, which consequently leads to substantial underestimation of hydrocarbon reserves (Davydycheva et al. 2017; Passalacqua et al. 2018). Investigations into the complex resistivity of shale samples by Yan et al. (2014) and Xiang et al. (2014, 2022) revealed that the organic-rich shale in southern China is characterized by low resistivity, high anisotropy, and high induced polarization, as opposed to the high resistance and polarization common in conventional HC reservoirs. Burtman et al. (2014) reached similar conclusions in their complex resistivity measurements of TerraTek shale rock samples. Moreover, during the hydraulic fracturing of shale gas reservoirs, the injection of thousands of tons of fracturing fluid into the reservoir results in the formation of low resistivity and high induced polarization anomaly bodies (Chen et al. 2000).

1.2 Challenges of CSEM Exploration Technologies

As the focus of oil and gas exploration transitions from conventional to unconventional exploration, EM exploration methodologies face significant challenges. Specifically, these challenges pertain to the tripartite geological problems of unconventional reservoir fluid identification, sweet spot detection, and reservoir parameter prediction. Consequently, there is a pressing need for continual innovation in the aspects of methodology, data acquisition, processing, inversion, and interpretation in order to augment the resolution and reliability of EM exploration approaches.

1.2.1 Inherent Limitations of EM Methods

The intrinsic disparity between EM and seismic techniques is rooted in their distinct field attributes. Seismic fields exist in the acoustic spectrum, while EM fields within lossy media are part of the diffusion spectrum; consequently, the resolution of EM methodologies is comparatively inferior to seismic. Low-frequency CSEM techniques, typically employed for oil and gas exploration, can readily be impacted by geometric effects, source imprint effects, and static shifts. Fortuitously, the evolution of high-precision 3D EM modeling techniques has delivered a potent mechanism to alleviate these detrimental influences. For example, the combined inversion of multiple field sources can efficaciously mitigate the field source effect (He 2019; He et al. 2021). The application of fictitious wave transformations to transient EM fields enhances interpretive reliability and the resolution ratio (Chen et al. 1999; Li et al. 2005; Mittet 2015, 2018; Stoffa and Ziolkowski 2018). The implementation of full zone, full coverage, full waveform field recording, uniform 3D EM data acquisition and processing, distinct wave field transformations, and inversion imaging techniques are critical for surmounting the inherent limitations of EM exploration methodologies.

1.2.2 EM Response Mechanism of HC Reservoir

The mechanism of EM response is intrinsically associated with the physical properties of reservoirs. Traditional EM methodologies grounded in the principles of EM induction and resistivity models encounter significant challenges when addressing the geological exploration and development issues inherent in unconventional oil and gas. A multi-parameter model that accounts for reservoir electrical anisotropy and the IP mechanism has emerged as a crucial theoretical tool for EM fluid identification and sweet spot detection (De Lima and Sharma 1992; Börner et al. 1996; Kavian et al. 2012; Fiandaca et al. 2012; Strack 2013). Given that the EM field of a horizontal electrical dipole encompasses both TE and TM components, grounded dipole CSEM is capable of measuring both horizontal and vertical resistivity. Consequently, WFEM, TFEM, LOTEM, and WEM methodologies offer substantial advantages for unconventional hydrocarbon exploration within highly anisotropic reservoirs. The characteristic time-domain and frequency-domain EM fields engendered by fluid and mineral presence in conventional oil and gas reservoirs have been extensively examined, resulting in the development of an equivalent complex resistivity model that accounts for EM induction, anisotropy and IP effects. Nevertheless, further research is required to elucidate the EM response mechanisms and interpretive modes of unconventional hydrocarbon reservoirs (Burtman et al. 2014; Burtman and Zhdanov 2015). To achieve precise multi-parameter joint detection of oil and gas, it is imperative to fully exploit the sensitivity of IP parameters within a complex resistivity model. Consequently, research focusing on the IP mechanisms and anomaly extraction methods within unconventional oil and gas reservoirs is essential to enhance detection accuracy and interpretive reliability. IP-based multi-parameter EM exploration methodologies have evolved into a focal point of research and represent the emerging trend in methodological development.

1.2.3 EM Data Acquisition

Exploration efficacy is largely contingent upon the spatiotemporal density and the quality of EM data, making data acquisition technique a vital prerequisite and guarantor

for the progression of EM exploration methodologies. Deep integration of methods, instruments, acquisition, and processing software is required in acquisition technology, considering factors such as field geology and terrain conditions, geological targets, among others. This necessitates feasibility analysis and simulation tests to establish an effective acquisition scheme. Primarily, substantial innovation in 3D acquisition is required within the acquisition method to attain multi-field source coverage, uniform illumination, and synchronize acquisition with several hundred thousand receivers to record substantial quantities of EM multi-component time-series data. This will satisfy the requirement of high spatiotemporal density data for high-precision inversion. Secondly, the development of high-quality acquisition and processing software capable of conducting noise level analysis, feasibility analysis, and data quality evaluation should be pursued to enhance exploration efficiency. Lastly, the manufacture of portable, intelligent, cost-effective, low power consumption, and low-noise multichannel receivers is essential to streamline the acquisition process.

1.2.4 CSEM Data Processing

Data processing serves as an integral constituent of the efficacious application of EM methodologies. Absent an appropriate data processing technique, the resultant findings would render futile, irrespective of the sensitivity of the instrument, the advancement of the acquisition techniques, and the high quality of data. Data processing chiefly comprises data preprocessing, attribute parameter delineation, and extraction. Noise reduction and correction signify the initial stage in data processing. Given the cultural noise and signal distortion instigated by the method or geological and topographical factors, specific noise reduction and correction techniques are requisite. Numerous contemporary signal processing techniques have been tailored to data noise reduction, including robust estimation, median filtering, wavelet transform, recursive filtering, and coherent analysis methods (Streich et al. 2011; Ji et al. 2016; Rasmussen et al. 2017; Wu et al. 2021). In contrast, correction techniques, such as source field and static shift correction, have been formulated in line with the attributes of the CSEM methods. Owing to the intricacy of CSEM methodologies and noise, there is an absence of universal correction and noise reduction techniques. The extraction of attribute parameters is certain to augment the reliability and impact of the inversion and interpretation. While DC and MT methods facilitate the definition of the apparent resistivity parameter, the complicated 3D attribute of the CSEM source imposes considerable challenges in defining the apparent resistivity. Hence, utilizing disparate field components or the combination of components of CSEM to define the attribute parameters via numerical computations, such as all-zone apparent resistivity, apparent polarizability, multi-frequency phase, oil–water identification factor, and differentially normalized factors, has garnered research interest, with several noteworthy application outcomes being achieved (Yan et al. 1999; He et al. 2015, 2021; Xue et al. 2020a, b).

1.2.5 CSEM Inversion and Interpretation Methods

Theoretically, every geophysical inversion embodies an underdetermined issue. It remains unachievable to infer precise information regarding subterranean anomalies from a single variety of geophysical data. Thus, an emergent research trend revolves

around comprehensive inversion and interpretation facilitated by multiple geophysical datasets. Joint inversion, incorporating as much prior information as available, serves as a proficient means to diminish inversion multiplicity, enhance data utility, and rectify inconsistencies in the inversion model. During the development phase of oil and gas fields, seismic and logging data are copious, prompting the joint inversion of EM, logging, and seismic data to garner research interest and yield superior specific results (Peng and Liu 2020; He et al. 2020). In unconventional oil and gas exploration, CSEM parameters, such as resistivity, polarizability, and anisotropy, exhibit sensitivity toward sweet spots, aligning with reservoir parameters like porosity, brittleness, permeability, and TOC. This forms a parameter foundation for reservoir prediction, thereby curtailing exploration and development risks. Joint inversion takes numerous forms, largely categorized into two classes. One stems from petrophysical relationships (Haber and Oldenburg 1997; Jegen et al. 2009; Heincke et al. 2010; Lelievre et al. 2012; Giraud et al. 2017; Astic and Oldenburg 2019; Peng et al. 2018; Hu et al. 2020; Xu et al. 2020; Yang et al. 2021a), while the other originates from structural similarity relationships (Gallardo and Meju 2003, 2004; Zhdanov et al. 2012; Lelievre and Farquharson 2013; Gao et al. 2017; Yan et al. 2020; Peng and Liu 2020). Structural coupling between EM and seismic has been applied (Mackie et al 2020). Research concerning the structural coupling algorithm primarily centers on the joint inversion of gravity, magnetic, and EM data, with structural coupling joint inversion employing seismic and EM data being a progressive trend in unconventional HC exploration. Due to the doubling of the parameters in anisotropic inversion and scarcity of observational information, numerous difficulties and challenges are presented in the inversion method to swiftly, accurately, and effectively ascertain the anisotropic information of oil and gas reservoirs (Liu et al. 2018).

1.3 Level and Ability of the CSEM Exploration Method

While the CSEM approach maintains a robust electrical foundation in unconventional HC exploration, the sweet spots of these unconventional HC reservoirs are characterized by substantial burial depths, diminutive targets, and potent heterogeneity. These attributes necessitate a heightened resolution, exploration depth, and an advanced degree of data processing and interpretation from the CSEM exploration methodology. Over the past two decades, there has been an all-encompassing enhancement of petroleum CSEM exploration methodologies. Considering the instrumentation, geophysical instrument corporations such as Phoenix, Zonge, KMS Technologies, Metronix, and Geonics offer high-power transmitters (exceeding 100 kW) and multi-functional networked portable receivers. The wide-frequency WFEM system, developed by China's Jishan High-tech company, the TFEM system created by BGP, CNPC, and the WEM system produced by the Institute of Geophysics, Chinese Academy of Sciences, have also been incorporated into oil and gas exploration (He et al. 2010, 2012; Di et al. 2016, 2019; He 2019). High-power transmitters can inject more than one hundred amperes underground, facilitating the emission of various waveforms, thus bolstering the source of CSEM. Receivers that are portable, lightweight, multi-functional, and distributed, with low power consumption, broad bandwidth, low noise levels, and large dynamic range, enable data acquisition for thousands of channel arrays. This offers a hardware assurance for 3D EM data acquisition and hydraulic fracturing monitoring under complex geological and terrain conditions. A plethora of

emerging CSEM methodologies in China are focused on improving resolution, detection depth, reliability, operational efficiency, cost, adaptability, and interpretation reliability, such as TFEM, WFEM, and WEM. The adoption of novel data processing, 3D inversion, and interpretation techniques has substantially amplified the capacity of CSEM methods to serve unconventional HC exploration.

2 Sweet Spot Interpretation Model and TOC Prediction

2.1 Models for Sweet Spot Detection

The traditional EM technique employs solely the resistivity parameter for the exploration and interpretation of oil and gas, resulting in considerable non-uniqueness and diminished reliability. The significance of the IP effect within rocks has been acknowledged, with efforts being made to incorporate both resistivity and polarizability parameters for the joint detection of oil and gas reservoirs (Davydycheva et al. 2006; He et al. 2010; Commer et al. 2011). The complex resistivity (CR) method, founded on the IP theory, has been utilized for over three decades in China for the identification of conventional oil and gas (Wu et al. 1996; Su et al. 2005). Two separate IP anomaly models were proposed to interpret the CR data. One, known as the micro-seepage model, assumes the IP effect occurs in the upper reducing zone where hydrocarbons migrate from the subterranean HC reservoir, culminating in the formation of a rich pyrite halo, which is the source of a potent IP effect, thus suggesting the HC reservoir exists directly beneath the IP anomaly (Oehler and Sternberg 1984; Veeken et al. 2009). Another model conceptualizes the electrical structure of an HC reservoir as a 'three-ring story', entailing a dynamic multiphase equilibrium system where a double electric layer forms in a biphasic medium, the source of IP, characterized by high resistivity and high induced polarization (He and Wang 2007). These two models have led to numerous favorable geological outcomes when applying the EM method in oil and gas exploration (He et al. 2005, 2010; Davydycheva et al. 2006). Shale gas, present in the reservoir either freely or in an adsorbed state, exhibits the typical attributes of self-generation, self-storage, and in situ accumulation, which necessarily predicates an IP anomaly interpretation model distinct from the previous two. The applicability of the above models to shale gas EM exploration, the geoelectric characteristics of organic-rich shale, the strength of the IP effect in a shale gas reservoir, and the integration of resistivity and polarizability for sweet spot identification, as well as the sweet spot detection pattern for CSEM exploration, remain open questions. Yan et al. (2014) and Xiang et al. (2014) gathered numerous shale samples from southern China and conducted complex resistivity measurements, discovering that organic-rich shale displays low resistivity and high induced polarization
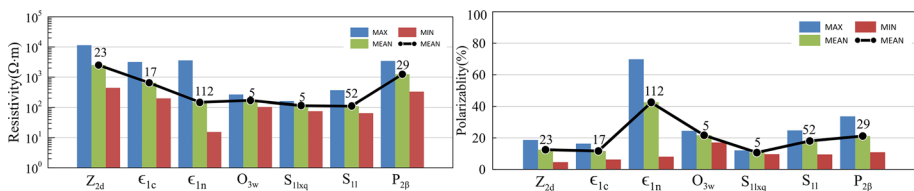

Fig. 1 Polarizability and resistivity results of complex resistivity measurement for geological outcrop rocks at different groups (Left: polarizability; Right: resistivity) (revised from Yan et al. 2014)

(Fig. 1). Further component analysis revealed an abundance of pyrite in organic-rich shale. Veeken et al. (2009) elaborated on the process and controlling factors of pyrite formation. The sedimentary environment of shale is a deep-water anoxic setting, essentially a reducing reaction environment. During the formation of secondary pyrite, organic carbon participates in the chemical reaction, acting as a catalyst. Thus, higher organic carbon content leads to an abundance of pyrite. The process unfolds as follows:

$$CH_4 + Ca^{2+} + SO_4^{2-} \rightarrow CaCO_3 + H_2S \uparrow + H_2O$$
$$H_2S + Fe^{2+} + 2OH^- \rightarrow FeS_2 + H_2O, \tag{1}$$
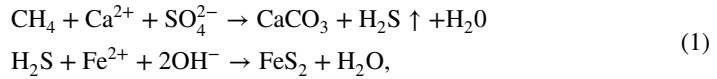
Furthermore, biodegradation and bacterial activity may contribute to the genesis of organic-derived pyrite within the sedimentary stack. Geochemical evidence indicates that secondary pyrite enrichment correlates with the TOC in shale reservoirs, thus marking pyrite as a telltale mineral of IP. Following the CR testing and analysis of unconventional reservoir rocks, three key insights have emerged: Firstly, the induced polarization of the sweet spot primarily originates from electron-conducting minerals such as pyrite, with the IP mechanism being the electron polarization process. Secondly, the sweet spot region exhibits characteristics of high induced polarization and low resistivity. Lastly, the sweet spot zone, its IP anomaly, and resistivity anomaly are co-localized in space. Consequently, the geoelectric model of EM exploration for sweet spots was proposed (Yan et al. 2014), providing a theoretical foundation for the CSEM detection and comprehensive interpretation of shale gas sweet spots (Fig. 2).
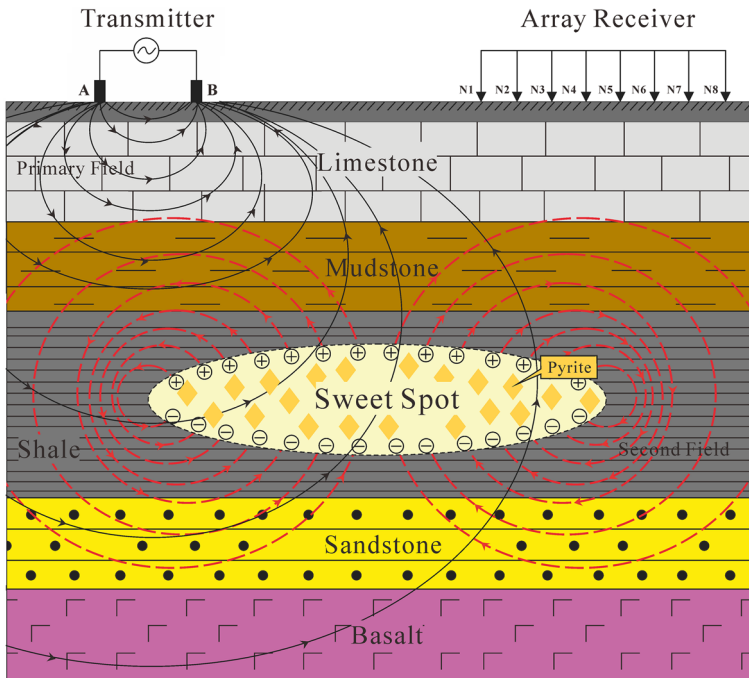

Fig. 2 Sketch map of geoelectric model for sweet spot detection. The central ellipse anomaly is with low resistivity and high polarizability
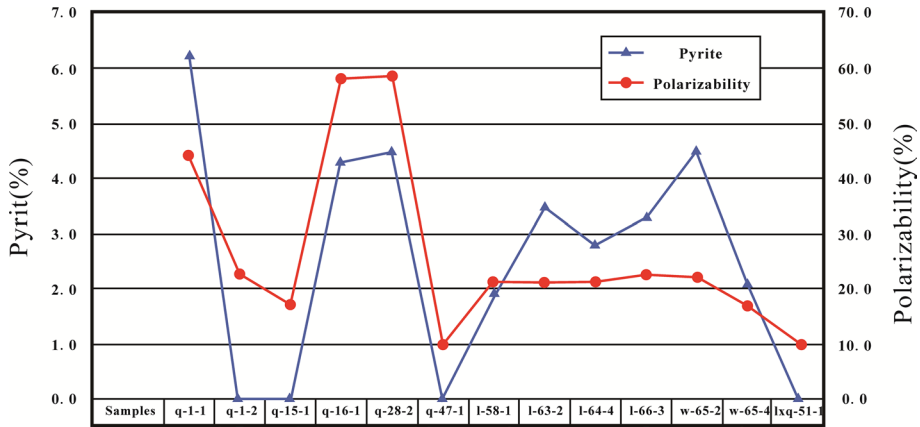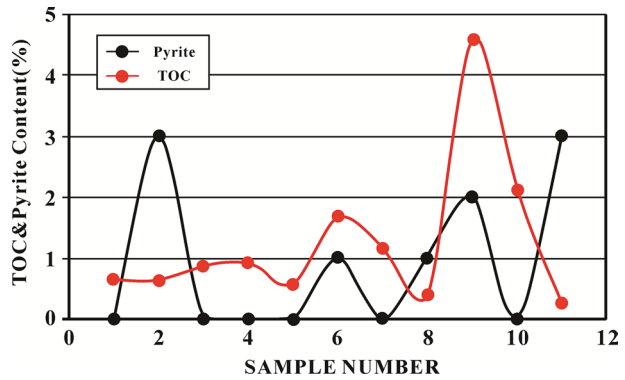
Fig. 3 Relationship between pyrite content and polarizability for rock samples (Yan et al. 2014)

Fig. 4 Relationship between TOC and pyrite and polarizability for rock samples (Yan et al. 2014)

2.2 TOC predicting

To explore the correlation between TOC, pyrite content, and the polarizability of organic-rich shale, 40 shale core samples from Well Zhao-104# situated in Southern Chongqing, and an additional 297 shale samples from the Upper Yangtze area were assembled (Zhang et al. 2013). Prior investigations by Zhang et al. (2013), Yan et al. (2014), and Xiang et al. (2016) targeted rock formations within the S_{1l}-O_{3w} and $Є_{1n}$ shale reservoir strata. As illustrated in Fig. 3, a positive relationship was found between polarizability and pyrite content. Figure 4 elucidates the relationship between TOC and pyrite content against polarizability, revealing a robust association between pyrite content and TOC.

Adao et al. (2016) conducted an analysis on low-maturity Posidonia shale rock samples from Northern Germany, finding a linear correlation between resistivity and TOC, with high resistivity as a notable characteristic (Fig. 5). This finding presents a stark contrast to the electrical characteristics of organic-rich shale in Southern China. Xu et al. (2020), through component analysis and complex resistivity inversion of shale samples from Southern China, discovered an exponential relationship between TOC and polarizability, resulting in the establishment of an empirical model (Fig. 6). Evidently, the construction of
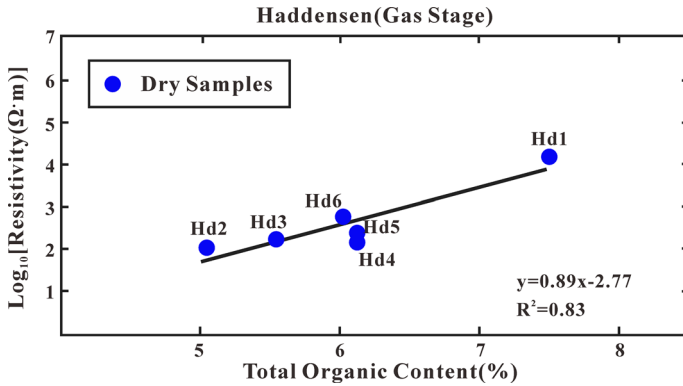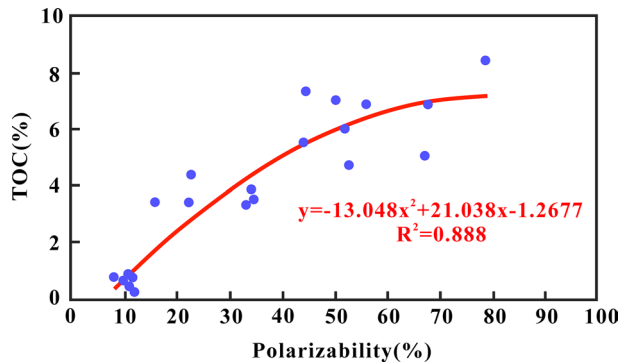
Fig. 5 Relation between electrical resistivity and TOC for Haddessen samples (dry condition) (Adao, 2016)

Fig. 6 Relation between the TOC and polarizability of shale samples (Xu et al. 2020)

a TOC prediction model is constrained by geological conditions, leading to the creation of disparate models in varying regions.

3 New Techniques in the Land Based CSEM

3.1 Definitions of EM Property Parameter

3.1.1 Models for EM Property Parameter Definition

EM theory elucidates that the attenuation of the electric dipole field with increasing distance proceeds at a slower rate than that of the magnetic dipole field. Additionally, the field conveyed by a horizontal electric dipole possesses TE and TM polarization modes within a layered Earth, whereas a large loop source maintains only a TE polarization mode. This characteristic endows the terrestrial line source with superior exploration depth and enhanced detection capabilities for thin resistive layers and anisotropy (Strack 2013). Consequently, the grounded line CSEM method has found broader application in the exploration of HC reservoirs and deep geological structures. Typically, the observed components encompass the horizontal electric field, vertical magnetic field, or the induced electromotive force. In surface

electrical investigations, explanatory parameters such as apparent resistivity are generally defined utilizing a half-space model characterized by uniform isotropic resistivity. However, as methodological research has deepened, observation technologies have improved, and new geological requirements have emerged, definition methods based on the polarized model and large-scale Earth model have become areas of significant research interest.

Figure 7 delineates three distinct models for definition. Figure 7a illustrates a half-space model with isotropic resistivity, which is utilized in the definition of apparent resistivity and phase in DC, MT, and CSAMT. Figure 7b portrays a half-space model with isotropic resistivity and polarizability, which is employed in defining apparent IP parameters in IP methods. Figure 7c represents the Earth-ionosphere model, which is applied in defining apparent resistivity and phase in WEM.

For the uniformly conductive and non-polarized half-space model, the time-domain electric and magnetic fields of the electric dipole are expressed as follows (Piao 1990):

$$E_x = \frac{P_E \rho}{2\pi r^3}\left[\Phi(u) - \sqrt{\frac{2}{u}}ue^{-u^2/2}\right], \tag{2}$$

$$\frac{\partial H_z}{\partial t} = \frac{3P_E \sin\theta}{2\pi\mu_0 r^4}\left[\Phi(u) - \sqrt{\frac{2}{\pi}}u\left(1 + \frac{u^2}{3}\right)e^{-u^2/2}\right], \tag{3}$$

where P_E is the moment of an electric dipole, ρ is the resistivity of the homogeneous half-space, $u = \sqrt{\frac{\mu_0}{2\rho t}}r$, r is the offset, t is the observation time, and $\Phi(u) = \sqrt{\frac{2}{\pi}}\int_0^u e^{-x^2/2}\mathrm{d}x$.

The electric and magnetic fields of the horizontal electric dipole in frequency domain are expressed as follows:

$$E_x = \frac{P_E \rho}{2\pi r^3}\left[3\cos^2\phi - 2 + (1 + ikr)e^{-kr}\right], \tag{4}$$

$$H_z = -\frac{3P_E \sin\phi}{2\pi k^2 r^4}\left[1 - e^{ikr}\left(1 + ikr - \frac{1}{3}k^2 r^2\right)\right], \tag{5}$$

where $k = \sqrt{-i\omega\mu/\rho}$, ϕ is the angle between the x-axis direction and $\vec{r}$.
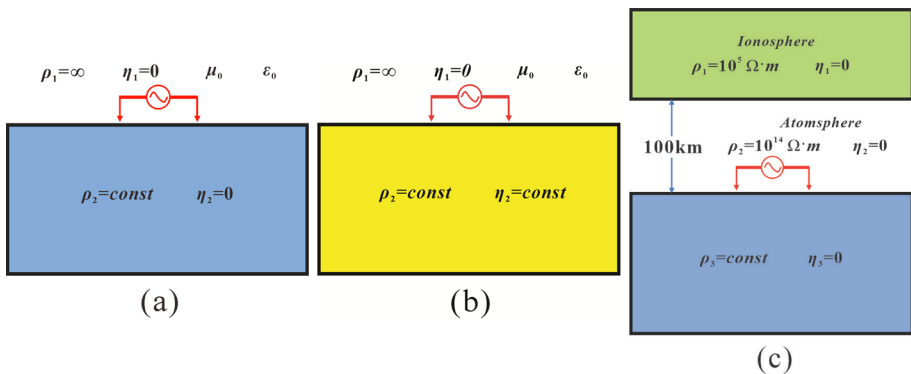

Fig. 7 **a** Conductive non-polarized half-space model; **b** conductive polarized half-space model and **c** the earth-ionosphere model

For the uniformly conductive and polarized half-space model, the time-domain electric field of the horizontal electric dipole can be written as follows (Davydycheva et al. 2006):

$$
E_x(t) = \frac{P_E \rho}{2\pi r^3} \left\{ \left[\mathrm{erf}(u) - \frac{2u}{\sqrt{\pi}} e^{-u^2} \right] + \eta e^{\frac{n^2}{u^2}} \left[1 - \mathrm{erf}\left(\frac{n}{u}\right) \right] \right.
$$
$$
\left. + \eta \left[\mathrm{erf}(u) - \frac{2nu}{\sqrt{\pi}} \right] e^{-u^2} + \eta e^{\frac{n^2}{u^2}} e^{2n} \left[1 - \mathrm{erf}\left(\frac{n}{u} + u\right) \right] \times \left(1 - 2n + 2n^2 \right) \right\},
\tag{6}
$$

where $n = 0.5\sqrt{\mu u r/(2\pi\rho)}$, erf (x) is error function.

For the earth-ionosphere model, the EM components of the ground source in frequency domain are written as follows (Li et al. 2015):

$$
E_x = i\omega\mu \frac{P_E}{4\pi} \int\limits_0^\infty F \cdot J_0(\lambda r) d\lambda + \frac{i\omega\mu}{k_1^2} \frac{P_E}{4\pi} \cos^2\theta \int\limits_0^\infty \left(FF - \frac{k_1^2}{\lambda^2} F \right) \cdot \lambda^2 \cdot J_0(\lambda r) \mathrm{d}\lambda
$$
$$
+ \frac{i\omega\mu}{k_1^2} \frac{P_E}{4\pi} \frac{1}{r} \left(1 - 2\cos^2\theta \right) \int\limits_0^\infty \left(FF - \frac{k_1^2}{\lambda^2} F \right) \lambda \cdot J_1(\lambda r) \mathrm{d}\lambda
\tag{7}
$$

$$
H_y = \frac{P_E}{4\pi} \int\limits_0^\infty -\frac{u_1}{R_1(0)} F \cdot J_0(\lambda r) \mathrm{d}\lambda
$$
$$
+ \frac{P_E}{4\pi} \frac{1}{r} \left(1 - 2\cos^2\theta \right) \int\limits_0^\infty \left[-\frac{R_1^*(0)}{u_1} FF + \frac{u_1}{R_1(0)} \frac{1}{\lambda^2} F \right] \cdot \lambda \cdot J_1(\lambda r) \mathrm{d}\lambda
\tag{8}
$$
$$
+ \frac{P_E}{4\pi} \cos^2\theta \int\limits_0^\infty \left[-\frac{R_1^*(0)}{u_1} FF + \frac{u_1}{R_1(0)} \frac{1}{\lambda^2} F \right] \lambda^2 \cdot J_0(\lambda r) \mathrm{d}\lambda,
$$

where F and FF are related to the electric properties of the ionosphere layer (Li et al. 2015).

3.1.1.1 EM Property Parameters Definition Examining Eqs. (2) through (8), it is evident that the interrelationship between EM field components and resistivity or polarizability is intricate. Constructing a display function for resistivity or polarizability is a complex endeavor, rendering the articulation of apparent resistivity and apparent polarizability via analytical expressions—as is done for apparent resistivity in DC and MT—unfeasible. Only through near-field or far-field approximation can expressions for near or far-field apparent resistivity and apparent polarization be articulated. This requirement constrains the exploration area to the data acquisition area and presents significant challenges in CSEM data processing and interpretation.

To derive effective EM property parameters, definitions are primarily approached from two perspectives. The first involves a numerical definition of all-zone apparent resistivity. The second strategy utilizes the parameter definition formula in DC and CR methods to define apparent resistivity, apparent polarizability, and the percent frequency effect. As a result, new CSEM exploration techniques with varying EM property parameters have been conceived. He (2010) advanced WFEM through defining all-zone apparent resistivity

based on Eqs. (4) and (5). This method integrates the near region, the transient zone, and the far zone, mitigating data distortion within the transient zone and broadening the CSEM exploration area. Furthermore, this definition has been incorporated into LOTEM and WEM, grounded in Eqs. (2), (3), and (8), thereby considerably enhancing the interpretation and application of data (Yang 1986; Yan et al. 1999; Xue et al. 2020a, b). TFEM merges frequency-domain exploration with time-domain exploration, establishing a time–frequency joint exploration method. This approach allows for the selection of different frequency current waveform excitations, depending on the target's depth. Via data processing and EM property parameter definition, not only can resistivity information be procured, but also IP information can be extracted, encompassing dual-frequency amplitude, dual-frequency phase, triple-frequency phase, and apparent chargeability (He et al. 2020, 2021):

$$\Delta A(\omega_i) = \frac{A(\omega_i) - A(\omega_{i3})}{A(\omega_i)}; \; \Delta\Phi_2(\omega_i) = \frac{\omega_{i3}\Phi(\omega_{i1}) - \omega_i\Phi(\omega_{i3})}{\omega_{i3} - \omega_i};$$

$$\Delta\Phi_3(\omega_i) = \Phi(\omega_i) - \omega\frac{\mathrm{d}\Phi(\omega_i)}{\mathrm{d}\omega} + \frac{2}{3}\omega^2\frac{\mathrm{d}^2\Phi(\omega_i)}{\mathrm{d}\omega^2}; \; M_s = \frac{\frac{1}{t_m - t_{m-1}}\int_{t_{m-1}}^{t_m}\varepsilon(t)\mathrm{d}t}{\varepsilon_0}, \tag{9}$$

where ω_{i3} is the third harmonic frequency of the fundamental frequency ω_i, A and Φ represent the amplitude and phase of the fundamental wave, respectively, and ε_0 represents the initial potential, t_m and t_{m-1} represent the mth and $(m-1)$th observation time, respectively. The difference between the tm and tm-1 is the length of the mth observation time window, and $\varepsilon(t)$ is the potential decay curve of potential with time t. Based on the above four TFEM property parameters, He et al. (2021) also defined the IP attribute anomaly parameter, realizing the quantitative identification of HC in reservoirs, this parameter is defined as follows:

$$Y_{L,i} = \frac{\eta_{L,i} - Q_L}{Q_L}, \tag{10}$$

where L is the type of TFEM property parameter, i is the number of measuring site, $\eta_{L,i}$ is the measured value, and Q_L is the threshold value obtained after observation at a known HC reservoir.

3.2 Pseudo-Random Waveform Technique

As an emerging technology for signal enhancement and noise reduction, PRBS has been initiated within the realm of CSEM exploration methodologies, primarily manifesting in two key applications. Firstly, in time-domain EM techniques such as LOTEM and MTEM, the source's transmitted current waveform adopts numerous broadband pseudo-random M sequences. Through conducting a cross-correlation between the M-sequence signal and the observed CSEM field component, noise can be effectively eliminated, thus procuring an earth impulse response with a superior signal-to-noise (S/N) ratio (Zhao et al. 2006). Consequently, apparent resistivity can be derived, facilitating the establishment of a transient electromagnetic method predicated on the earth impulse response (Ouyang et al. 2019). Drawing from the half-space model, Yuan et al. (2018) simulated the cross-correlation process between the current waveform and the received EM signal, thereby obtaining the earth impulse response. Figure 8 delineates three M-sequence signals varying in frequency band and length, along with three corresponding voltage responses. Figure 9 exhibits three
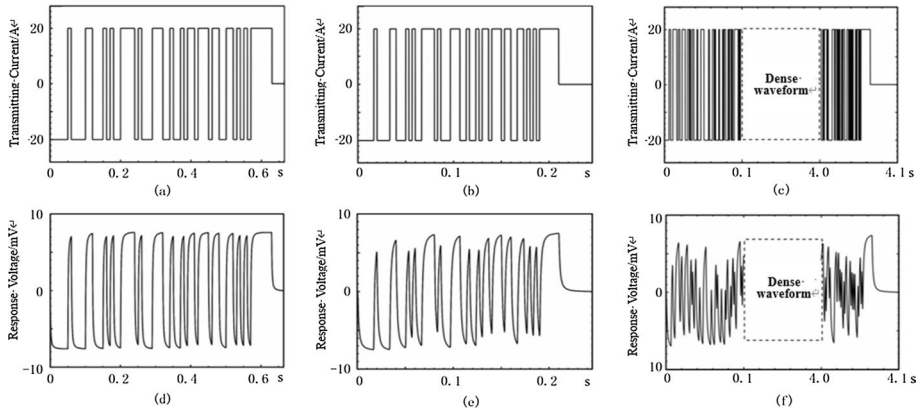
Fig. 8 Transmitted and received waveforms corresponding to three groups of coding parameters in a noiseless environment with different frequency bands. **a–c** are three different coded transmission current waveforms. **d–f** are the corresponding voltage responses, respectively (Yuan et al. 2018)
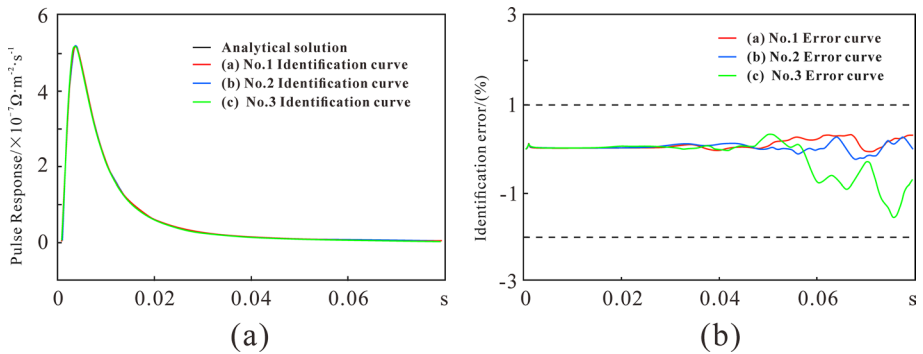

Fig. 9 **a** Correlation impulse response and, **b** impulse response errors corresponding to three groups of coding parameters in a noiseless environment (Yuan et al. 2018)

impulse responses and corresponding errors, derived from the cross-correlation between the M-sequence signals and the voltage responses. These responses are in alignment with the impulse response of the homogeneous half-space earth model. The error curves suggest that the broader the frequency band of the current M-sequence waveform, the greater the accuracy of the obtained earth impulse response. Wang et al. (2016) and Streich et al. (2011) applied the MTEM methodology, underpinned by PRBS, to terrestrial oil and gas exploration, substantially improving the quality of observation data and achieving commendable geological results in the detection of high-resistance reservoirs.

Another application of PRBS involves the deployment of a pseudo-random seven-frequency waveform (2^n sequence, with n ranging from 0 to 7). Frequency response characteristics demonstrate that the base frequencies of the 2^n sequence waveform are uniformly distributed along the logarithmic frequency axis, exhibiting essentially identical amplitudes and initial phases (Fig. 10). Evidently, a solitary transmission of the pseudo-random seven-frequency waveform can facilitate the observation of seven spectral signals with an elevated S/N. WFEM leverages this waveform to actualize a broadband, multi-frequency
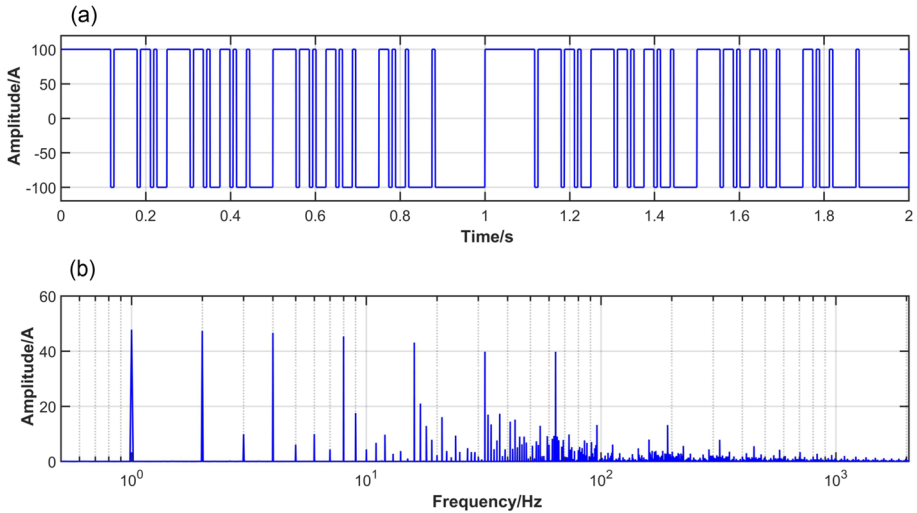
Fig. 10 The pseudo-random seven-frequency waveform (A = 1, T = 1 s), **a** is the time-domain waveform, and **b** is the spectrum (Yang Y et al., 2021)

signal configuration, thus optimizing transmission and reception efficiency, bolstering resistance to noise, and ensuring data quality (He 2010; Jiang 2010; Yang et al. 2021b).

3.3 Utilization of the Sky Wave

Based on modeling of field components for varying lengths of wire source at different frequencies, as illustrated by Eqs. (9) and (10), Di et al. (2008) and Li et al. (2015) deduced that once the source length is commensurate with the height of the ionosphere, the influence of the skywave (waveguide) warrants consideration. As depicted in Fig. 11, the electric field on the surface, computed based on the earth-ionosphere model, exceeds that of the homogeneous half-space model when the transmitter to receiver distance (r) spans several hundreds of kilometers. This revelation led Di et al. (2008) to propose the concept of WEM. Figure 12 provides a schematic representation of the WEM operational principle. From the onset of this century, China embarked on the research and establishment of the
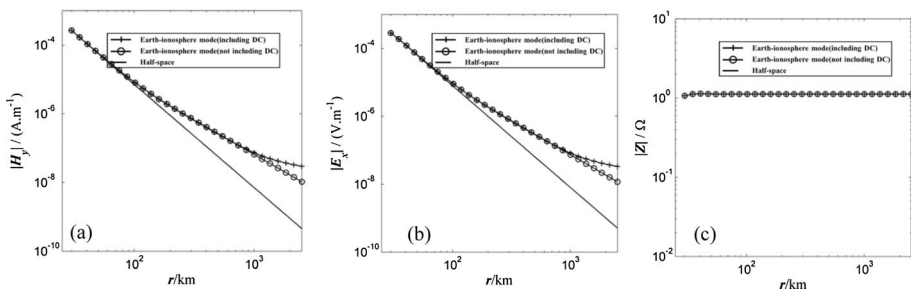

Fig. 11 **a** |Hy|, **b** |Ex|, and **c** |Z| field decay curves for axial array at 32 Hz (Li et al. 2015)
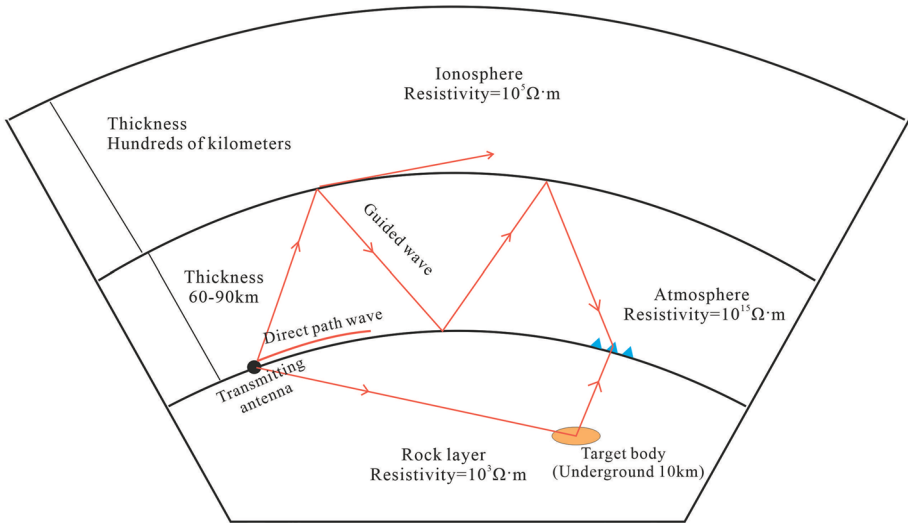
Fig. 12 EM waves propagation of WEM source (modified from Di et al. 2020)

'Extremely Low-frequency Ground Exploration Project,' culminating in the construction of a fixed tensor source spanning over 100 km in Central China. The transmission power reaches up to 500 KW, with a peak current of 150A. An EM field encompassing 21 frequencies, ranging from 0.1 to 300 Hz, is transmitted. Owing to the existence of a waveguide field, the WEM signal can be effectively observed at considerable distances against the MT background (Fig. 13), blanketing the Chinese mainland area. The quality of the WEM curve markedly surpasses that of the MT data (Fig. 14), a factor of substantial theoretical and practical significance for EM exploration in mainland China.
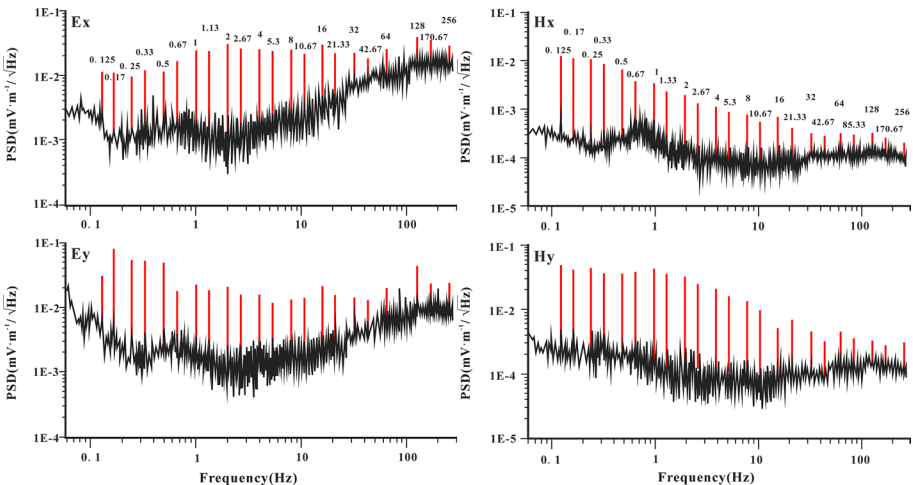

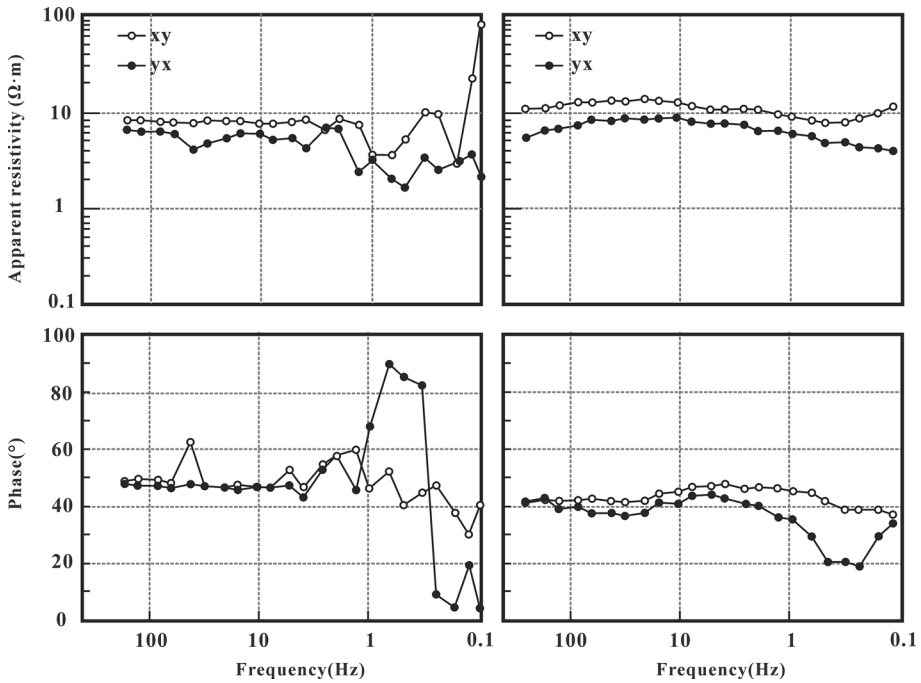**Fig. 13** Comparison of power spectral density between WEM and MT fields (Zhuo et al. 2007)

Fig. 14 Comparison of apparent resistivity and phase curves between MT (left) and WEM (right) at site 31(Zhuo et al. 2007)

3.4 Remote Reference and Array Data Processing Techniques in CSEM

Besides traditional strategies of amplifying the current, increasing stacking times, and extending observation time to enhance the S/N of data, the application of CSEM remote or/and near reference observation and processing technology also serves as a crucial element for data quality improvement. Strack et al. (2008), Allegar et al. (2008), Stephan and Strack (1991) successfully implemented local noise compensation technology (LNC) in the LOTEM method, attaining a substantial noise reduction effect. Yan et al. (2012) introduced the near-reference magnetic field observation and processing technology for CSAMT. With the growing trend of distributed design, array measurement, and synchronous acquisition of regional data, the temporal-spatial characteristics of array data facilitate reference processing technology. Zhou et al. (2019) put forth a space–time array mixed-field source electromagnetic method grounded on multi-input and multi-output system analysis. By synchronously processing the array data observed by multiple stations, superior quality EM data for MT and CSEM can be achieved, while concurrently suppressing relevant noise. For denoising processing in LOTEM data, a combination of LNC and the variational mode decomposition (VMD) technique was proposed. This combination effectively mitigates the noise in time-domain EM data and enhances the decay curve quality. Figure 15 presents the raw data at site S1 across four successive cycles, pre- and post-stack processing decay curve, and the LNC + VMD processing decay curve of the secondary Ex. From the comparison, it is evident that the
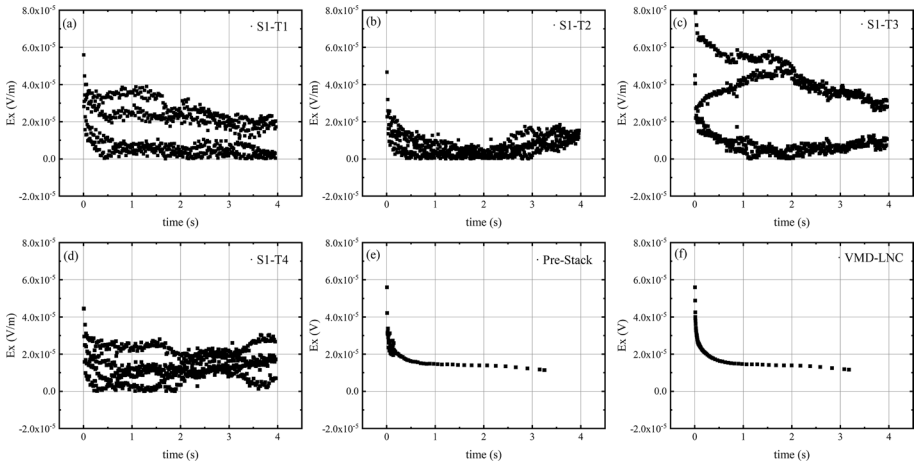
Fig. 15 LOTEM noise removal effect. (**a–d**) are four-period data observed in suburban area, **e** is the decay curve with pre- and post-processing, and **f** is the decay curve with LNC + VMD

quality of the initial part of the curve has considerably improved, with the tail transitioning to exponential decay, rendering it more logically sound.

3.5 Model Space-Constrained Inversion

Diverse geophysical methods extract physical property data of geological entities from distinct perspectives. However, due to the profound non-uniqueness inherent to individual inversions, geological models deciphered through different geophysical methods can substantially differ, even to the point of incompatibility. To ameliorate resolution and diminish non-uniqueness, the most efficient approach is multi-method and multi-observation field joint inversion, underpinned by prior information (Liu et al. 2021). He et al. (2020) formulated a joint objective function through TFEM multi-component data, and introduced a methodology to restrict parameter spaces of thickness, resistivity, and polarizability, utilizing seismic information and well logging. By integrating the artificial fish swarm algorithm and simulated annealing nonlinear algorithms with step-by-step constraint schemes, the non-uniqueness of inversion was successfully circumvented, thus assuring exploration precision and efficacy. Figure 16 presents the resistivity and polarizability profiles acquired through the constrained inversion of TFEM in the tight oil and gas exploration context. During the inversion process, not only were seismic interfaces (indicated by the dashed line in the figures) taken into account as constraints, but also constraints based on logging and geological data, such as upper and lower boundaries of resistivity and polarizability, were applied. As discernible from Fig. 16 in the circled area, there exists lateral variation in resistivity and polarizability within the same stratigraphic layer, with a noticeable enhancement in the resolution of thin layers in the vertical direction. In the focal exploration segment (the circled area in Fig. 16), a medium resistivity and high polarizability anomaly was identified, attributed to a HC reservoir. Therefore, an increase in prior information directly correlates with the accuracy of the inversion of unknown physical parameters, amplifying the discriminative power for HC reservoir exploration.
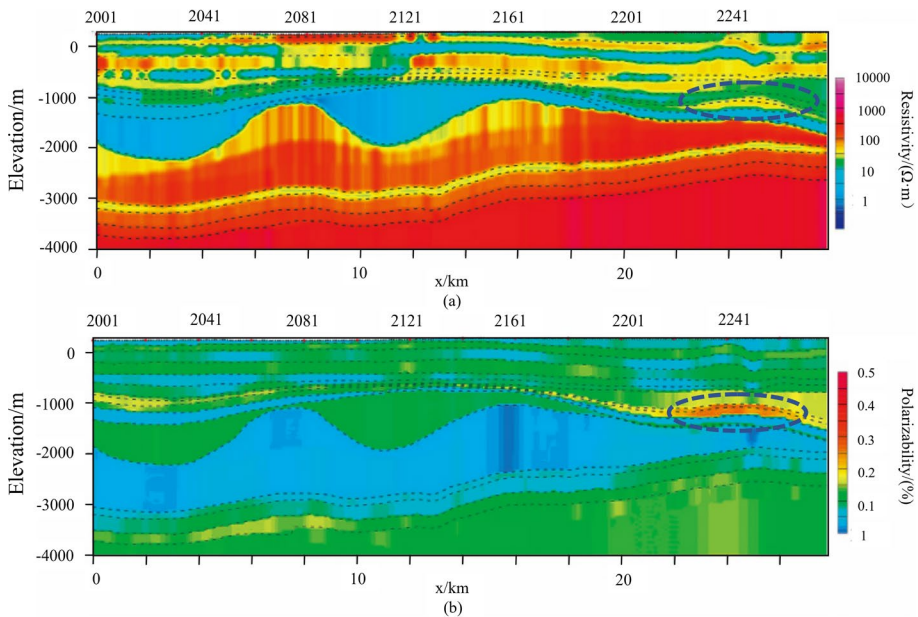
Fig. 16 Model space-constrained inversion profile of resistivity and polarizability (top: resistivity; bottom: polarizability; ``bullet'' The circled Area: anomaly in the target) (He et al. 2020)

4 Cases Histories

In this review, I will present three cases on shale oil exploration, shale gas sweet spot detecting, and hydraulic fracturing monitoring with WFEM, TFEM, and LOTEM methods (Zhang et al. 2013; Liu et al. 2015; Zhang et al. 2017; Yuan et al. 2017; Yan et al. 2018).

### 4.1 WFEM Application in Shale Oil Exploration

Situated in southern Jiangxi, China, the basin under discussion hosts a range of mud shale and oil shale formations including the Cretaceous, Permian, Silurian, and Cambrian. These formations are broadly distributed, exhibit considerable thickness, and possess relative stability. The oil shale target layer, denoted as k_{1b}, is predominantly found at a depth of approximately 1500 m, extending a thickness of around 200 m. This basin's seismic wave impedance contrast for shale oil reservoirs is mini-scale, the reflected energy is weak, and the scattering of seismic waves is considerable, which collectively make the detection of shale oil sweet spots via seismic methodologies challenging. Table 1 provides the statistical analysis of the lithology and resistivity of stratigraphic samples. As per the data in the table, the resistivity of the oil shale layer is roughly 100 Ω m, about a fifth of the resistivity exhibited by the surrounding rocks, signifying a conspicuous electrical difference. Remarkably, the overall resistivity of the oil shale electrical model greatly surpasses that of the shale gas electrical model (with resistivity of organic-rich shale strata under 10 Ω m), suggesting that the CSEM exploration depth in oil shale exploration significantly exceeds that of shale gas exploration. To illuminate the electrical characteristics of the source rocks,

Table 1 Statistical results of lithology and resistivity for the basin (Zhang et al. 2017)

Stratum	Main lithology	Thickness(m)	Resistivity ($\Omega \cdot$m)	Electrical characteristics
K_2g	Fine sandstone, sand mudstone,	700	200	Intermediate resistivity
K_2z	Sandstone, Glutenite,			
K_2m	Conglomerate, Glutenite	300	500	Secondary high resistivity
K_1l	Siltstone, Tuffaceous			
K_1b	Oil shale, Mud shale, Marl	200	100	Low resistivity
K_1b	Breccia lava, Siltstone,	500	500	Intermediate resistivity
K_1j	Rhyolitic brecciated tuff		1000	High resistivity
J_1l	Sandstone			

establish a theoretical foundation for geological appraisal, and pinpoint drilling locations, a research collective from Central South University conducted WFEM exploration in this region. Initially, the feasibility of WFEM exploration was scrutinized. Two distinct models were crafted based on the geoelectrical parameters outlined in Table 1. One model corresponds to a target layer containing oil shale with a resistivity of 100 Ω m, which is approximately 20 times more resistive than 95% of the world's hydrocarbon provinces (between 3 and 35 Ω m), while the other model represents a target layer devoid of oil shale and exhibiting a resistivity of 500 Ω m. Figure 17 displays the WFEM forward results, with the blue and red curves in the figure corresponding to the apparent resistivity curves of the models inclusive and exclusive of the oil shale layer, respectively. Notably, a significant difference can be observed between the two curves when the frequency is less than 300 Hz, with the maximum abnormal relative change reaching 60%. This suggests the feasibility of identifying shale oil anomalies in the reservoir by interpreting the WFEM apparent resistivity curve.

The WFEM survey was conducted along the NNW trajectory, orthogonal to the regional tectonic orientation. The entire line spans a length of 9 km, with measurements taken at 100 m intervals. Notably, an intensified measurement was executed along the middle section of the line, where the intervals were condensed to 50 m. To achieve the proposed exploration depth and conform to efficiency requisites, the transmitted waveform was
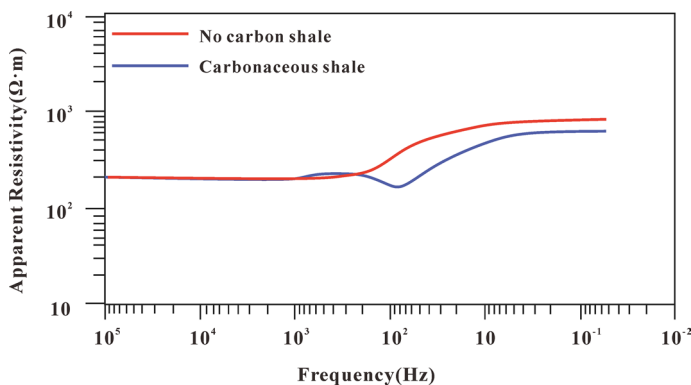
Fig. 17 1D apparent resistivity curves for shale scenarios with and without oil- gas shales layers (Zhang et al. 2017)

generated as a 2^n series pseudo-random signal containing seven distinct frequencies. The frequency range encompassed in the measurements was broad, ranging from 0.01 to 8192 Hz, with a total of 40 frequency points. The terrestrial source, labeled AB, extended over a length of 1.3 km, emitting a current of 120 A. The transmission-reception distance fluctuated between 16.0 and 17.25 km, and the maximum observation angle—delineated as the angle between the line drawn from the survey line's starting point to the midpoint of the transmitting source and the line drawn from the survey line's endpoint to the transmitting source's midpoint—amounted to 22°. Precise line design, accompanied by optimized observation parameters, assured the high-quality acquisition of WFEM observational data. Figure 18a presents a cross-section illustrating the 2D resistivity inversion profile, paired with a geological interpretation. The resistivity profile appears segmented into three distinct lateral sections: the southeastern segment (extending from site 101 to site 126) exhibits a resistivity profile characterized by a high-low-high distribution from the surface to the subsurface strata; the middle segment (ranging from site 126 to site 170) displays a top-to-bottom resistivity pattern of low-high-low; lastly, the northwestern segment (from site 170 to site 195) echoes the high-low-high distribution evident in the southeastern section. Overall, the survey line delineates a faulted basin demonstrating a northeastern dip. Strata at the terminal points of the survey line are elevated, while those located centrally manifest an overall depression. This depression houses a broad, gently arcing anticline within the Cretaceous strata, ranging from site 126 to site 160. Meanwhile, the result also uncovers a concentrated fault structure prominently developed at the extremities of the profile. The primary faults F70 and F26, constituting reverse faults, are situated at the northern and southern termini of the fault basin. These fault lines govern the shale formation at the southern terminus of the profile. The Banshi Formation incorporates oil shale, mudstone, shale, and other organic-rich source rocks, which are autochthonous and self-storing, thereby constituting favorable reservoirs for shale oil. These are detected as conductive anomalies with an approximate depth of burial at 1300 m.

The fault structure observed in the middle of the survey line demarcates an advantageous region for shale oil exploration, given its moderate depth of burial and desirable continuity of the target layer. The apparent polarizability profile, displayed in Fig. 18b, discloses a high induced polarization zone extending from site 116 to site 170. The cumulative interpretation of resistivity and polarizability posits the shale oil anomaly between site 126 and site 170, with a burial depth ranging from 1000 to 1600 m and an average thickness of 560 m. Well No.1 is strategically situated between site 142 and site 143, as indicated in Fig. 19, which presents a depth histogram of the lithological strata. The respective burial depths of the Guifeng Formation, Zhoutian Formation, and Maodian Formation are discerned at 116 m, 466.53 m, and 924.46 m. The depths of three interfaces, interpreted based
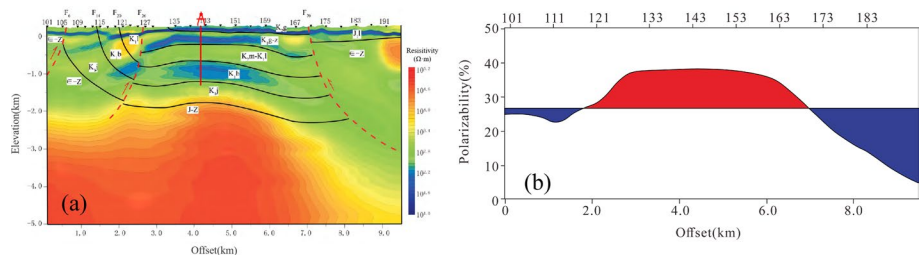

Fig. 18 **a** Profile of the 2D resistivity inversion and geological interpretation, and, **b** the profile of the apparent polarizability curve (Zhang et al. 2017)

Stratum	Histogram	Lithology	Depth(m)
K$_2$g		Fine sandstone Sand mudstone	— 116 —
K$_2$Z		Sandstone Glutenite	
K$_2$m		Conglomerate	—466.53—
K$_1$b		Oil shale Mud shale Siltstone	—924.46—

Fig. 19 Lithological log of the drilling stratum, lithology, and resistivity (Zhang et al. 2017)

on the resistivity profile, are observed at 155 m, 490 m, and 920 m. This concordance between the inversion depth and drilling results underscores the accuracy of the former. Furthermore, a two-meter-thick fractured oil shale layer was found in the Banshi Formation at a depth of 1500 meters. These findings corroborate the efficacy of jointly utilizing WFEM resistivity and polarizability in the detection of shale oil anomalies.

4.2 Shale Gas Sweet Spot Detection with TFEM

The Yangtze marine carbonates are well developed in Southern China, and its outcrops cover a series of strata from Quaternary to Presinian, forming a complex mountainous terrain. There are several sets of marine organic-rich shales. In Southern China, a large quantity of shale gas has been discovered in the black shales of the Niutitang group of Cambrian age, the Longmaxi group of Silurian age, and the Ordovician Wufeng group. The thickness of these three groups is 200–400 m, and the shale layers are rich in organics. The total organic carbon (TOC) content changes from 1.85 to 4.36%. 175 rock samples from the ground surface, and 18 rock cores from 3 wells collected in Zao Tong area were measured in laboratory. Table 2 shows that the shales have low density, low susceptibility, low resistivity and high polarization compared to the overlying and underlying layers. In terms of resistivity, the three sets of shale present low resistivity compared to sand, limestone and metamorphic lithologies—the obvious low resistivity target layers for EM methods. However, the most significant feature for shale is its high polarization, agreeing well with high TOC values of the samples collected from the outcrops, and those from wells Z104 and N201, which means that high organic content is the key factor resulting in high polarization for shale. The TFEM methodology was employed to examine organic-rich shales in Zao Tong, located in southwestern China, during the period of 2011–2013. Figure 20

Table 2 Physical properties of rock samples in Zao Tong, Southwestern China (Zhang et al. 2015)

| Geological Age code	Main lithology	Density (g/cm^3)	Susceptibility (10^{-5}SI)	Resistivity (Ω·m)	Polarization (%)	TOC (%)
Q				100–200		
T	Sandstone, limestone	2.65–2.74	25–93	100–200		
P	Shale, basalt	2.69–2.93	16–3800	1500–2000		
S	Shale, sandstone	2.40–2.63	15–27	100–150	17.5–24.8	2.94–8.75
O	limestone	2.7	3–20	1000–1500		
	shale	2.63		30–50	17.5–24.8	2.94–8.75
ϵ	limestone	2.69–2.73	17–33	1000–1500		
	shale	2.36–2.56		10	39.8–42.7	1.00–5.50
Z	Sandstone, dolomite	2.63–2.69	6–24	>2000		
	shale	2.21–2.29		20–45	16.7–25.4	>2
Pt	Metamorphic, slate	2.69	34	>2000		
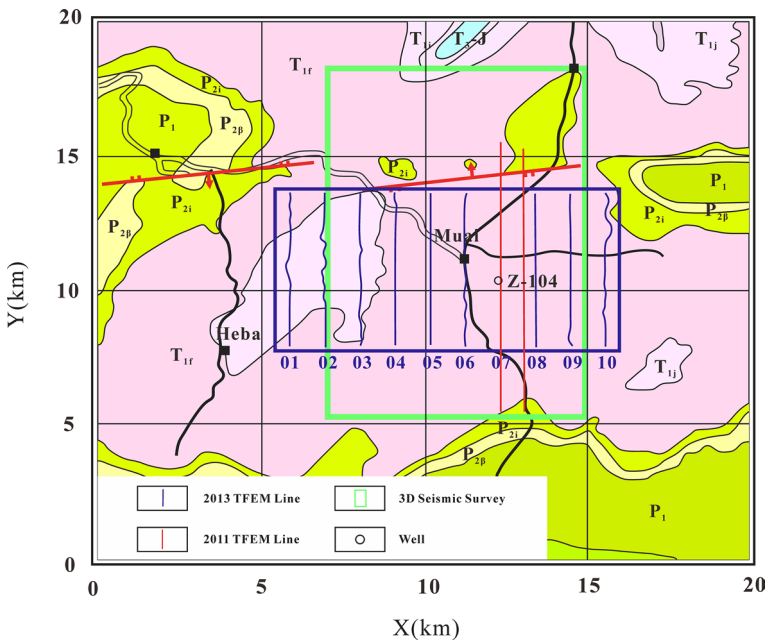
Fig. 20 Geo-map and survey lines of the TFEM Zao Tong area (Zhang, 2015)

illustrates the geological map along with the layout of the TFEM survey. The exploration region, covering an area of 60 km^2, is intersected by 11 lines spanning a total length of 71.3 km, with 724 sites positioned at 100 m intervals. The area's exploration encounters

a few challenges due to the high population density and the widespread presence of factories, coal mines, and metal mines, which generate a significant EM noise. Additionally, the surface is blanketed with carbonate outcrop of high resistivity, shaping a fluctuating terrain with an altitude difference of 500 m, adding complexities to EM sweet spot detection. To ensure a superior S/N during field data collection, a series of measures have been put into effect.

Firstly, a broad-range voltage and a constant, adjustable high-power current ensure a stable output exceeding 50 A. Secondly, the two extremities of the 5-km-long transmitting source are strategically positioned in low-lying wet regions according to the corresponding topography, achieving comprehensive coverage and enhancing work efficiency, thereby making it apt for regional exploration in geologically challenging areas. Finally, distributed wireless acquisition stations can be arranged in the receiving area, with offsets ranging from 2 to 10 km. The placement of these stations is determined flexibly, in accordance with the actual terrain conditions. Magnetic sensors are buried and covered with compacted soil to mitigate interference caused by wind.

The interpretation of TFEM data encompasses three distinct stages. Initially, data preprocessing is performed, which involves de-noising and normalizing the excitation current. Following this, double-frequency phase anomalies, apparent resistivity $\rho_a(t)$, and longitudinal conductivity $S(t)$ are qualitatively extracted, providing insights into the polarization properties of the rocks at each location. Subsequently, through constrained inversion, the resistivity and polarizability of the target layer are derived. Lastly, TOC is estimated using the inversion data and the relationship model between TOC, resistivity, and polarizability, which has been established through petrophysical studies. The spatial locations and attribute evaluations of sweet spots are provided, taking into account geological and seismic data. Figure 21 illustrates structural models constructed with seismic and inverted resistivity and polarization sections from Line 7. As displayed in the figure, two distinct sets of low resistivity layers, each with a thickness of approximately 200m, are clearly identifiable at depths of 2 km and 4 km, respectively. These shale layers pertain to the Silurian Longmaxi group-Ordovician Wufeng group and the Cambrian Niutitang group, respectively.

Through the examination of ten TFEM inversion profiles, Fig. 22a and b presents the planar views of polarizability and resistivity pertaining to the two reservoir layers. The delineation of regions rich in TOC—as discerned through resistivity and polarizability anomalies (Fig. 22a and b) along with the application of a TOC predictive model—is circumscribed and depicted in Fig. 22c. Notably, two extensive regions with high TOC values are discerned in the northwestern and eastern sectors of the test zone, covering a
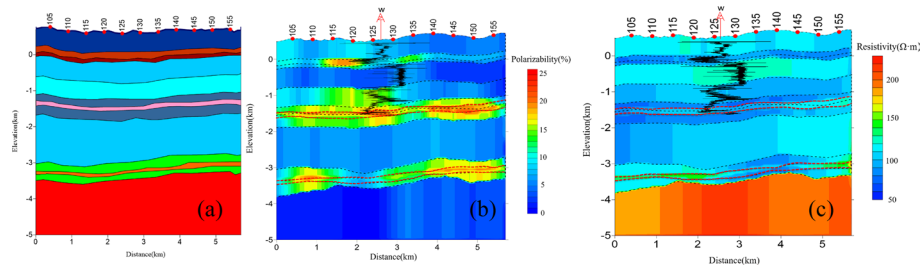

Fig. 21 a Initial model constructed by seismic result and **b** constrained inversion resistivity section and **c** polarization section of line 7. Logging data are also shown in (**b**) and (**c**) (Zhang et al. 2015)
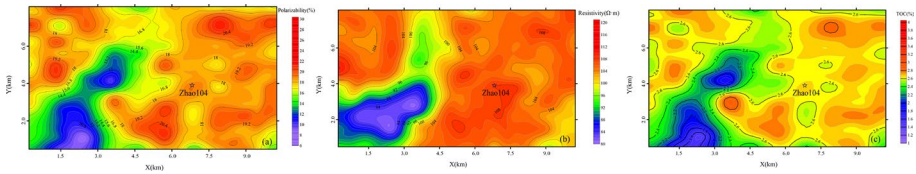
Fig. 22 3-D demonstration of (**a**) inverted polarization, (**b**) inverted resistivity, and (**c**) high TOC anomaly map of upper shale layer determined by integrated resistivity and polarizability anomalies

combined area of 45 km^2. The derived findings were subsequently leveraged to guide the development of shale gas resources. The ZT 104 borehole, along with subsequent drilling operations conducted within the predicted sweet spot zones, yielded industrially significant quantities of shale gas. Therefore, it can be posited that the TFEM method's ability to detect sweet spots within the two shale gas reservoirs has proven to be effective.

4.3 Application in Dynamic Monitoring of Hydraulic Fracturing

The Jiaoshiba shale gas field, located in the eastern periphery of Chongqing, represents the largest consolidated gas reserve in China. The pragmatic utilization of hydraulic fracturing technology acts as a catalyst in stabilizing and incrementing production within this region. Micro-seismic surveillance is of paramount importance in enhancing the effectiveness of fracturing operations. However, the intricate topography and surface geological circumstances prevalent in this territory exert a significant impact on the S/N and positioning precision of the micro-seismic technique. Additionally, inherent limitations within the micro-seismic approach result in an imprecise estimation of the effective reservoir volume (ERV) (Hoversten et al. 2015). It is widely recognized that upon the introduction of a considerable volume of fracturing fluid into the reservoir rock strata, the fluid propagates along the pre-existing microfractures, continuously widening the fracture network. This activity induces alterations in the electrical properties of the reservoir. Given the intrinsically low resistivity of the fracturing fluid and the enhanced connectivity stemming from the fracturing process, the stimulated reservoirs exhibit significantly diminished resistivity and elevated polarizability characteristics.

Therefore, the EM fracturing monitoring method is underpinned by a strong geophysical foundation. The application of the EM approach facilitates the acquisition of sensitive parameters including fluid trend, volume alteration, and interconnectivity, both during and subsequent to fracturing operations. This data serves as a critical determinant in making informed decisions regarding the optimal development of unconventional HC reservoirs.

4.3.1 Geoelectric Model

Table 3 represents the geoelectric model of the Jiaoshiba shale gas field, formulated based on the well logging of JIAOYE-1. The model reveals a notable concordance between resistivity, polarization, and geological formations. The resistivity of the shale is markedly less than the surrounding rock, and the organic shale within the reservoir is distinguished by elevated polarizability.

Table 3 Geo-resistivity model based on JIAOYE-1 Logging curve

Stratigraphy	Lithology	Depth (m)	Thickness (m)	Resistivity (Ω·m)	Polariz-ability (%)
P_{2ch}-C_{2hl}	Limestone	0~1430	1430	>2000	
S_{2h}-$S_{1l\text{-}up}$	Mudstone	1430~2290	860	30–40	
$S_{1l\text{-}up}$	Sandstone	2290~2330	40	244	10
$S_{1l\text{-}low}$ -O_{3w}	Gas-bearing shale	2330~2410	80	42	20
O_3-O_1	Limestone	2410~		>1000	

4.3.2 Normalized Double Difference Residual (NDDR) Technology

The four-dimensional (4D) processing methodology is conceived, grounded on the geoelectric model of the Jiaoshiba shale gas field. An approach identified as Normalized Double Difference Residual (NDDR) was innovated for the processing of LOTEM 4D data. The technique for the measurement and computation of the NDDR parameter is illustrated in Fig. 23, employing the Jiaoshiba geoelectric model (Table 3) to authenticate its effectiveness. In the model, the resistivity of the shale reservoir is presumed to be 42 Ω m prior to fracturing, and 5 Ω m subsequent to fracturing. The Ex-curves are represented in Fig. 24a. The figure demonstrates that when reservoir fracturing is executed at a depth of 2330 m, the electric field between the decay time of 5 ms to 100 ms exhibits substantial changes, and the appearance of an 'X' cross symbol in the curves is noticeable. To emphasize the alteration in the Ex-field induced by fracturing, within the log–log domain, the NDDR parameter is determined as follows:

$$DF_{Ex} = 100 \times d \big| [\log \Delta E_x(t1)] - \log[\Delta E_x(t2) \big| / d \log[\Delta E_x(t1)], \tag{11}$$

where DF_{Ex} is the value of normalized residual, ΔE_{x1} is the rate of E_{x1} change over t_1 period before fracturing, ΔE_{x2} is the rate of E_{x2} change over t_2 period after fracturing. Figure 24b is NDDR curve according to Eq. (11) and the Ex-data of Fig. 24a , which can be
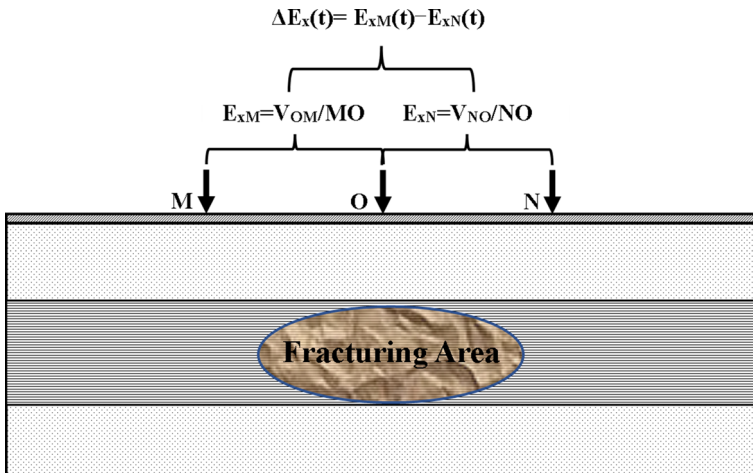

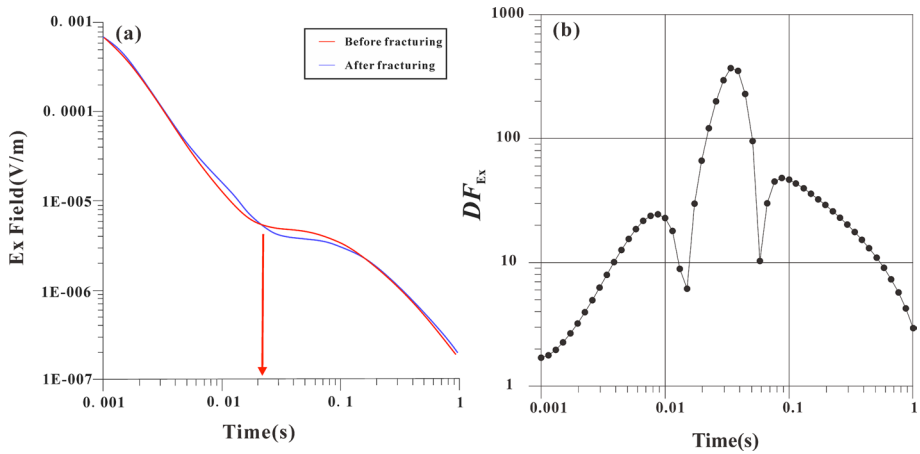**Fig. 23** The schematic diagram of measuring and calculating the NDDR parameter

Fig. 24 **a** The EM field before/after fracturing and, **b** NDDR curve based the geoelectric model (Yan et al. 2018)

seen that the response time of fracturing is in the range from 30 to 40 ms, the accuracy of the time window improves so much.

4.3.3 LOTEM Monitoring and Analyzing

In the year 2017, the EMLAB assembly of Yangtze University deployed the LOTEM technique for ongoing fracturing surveillance examinations in the Jiaoshiba shale gas field. A total of 8 lines, each spanning 1400 m, and 224 sites with 50 m intervals, were established atop the 6th, 7th, and 8th stages of the horizontally hydraulically fractured well. The ground source extends 4000 m east–west, transmitting a bipolar square wave with an 8 s period and 50% duty cycle at 65 A output. The minimum offset measures 5000 m, with a 400 Hz sampling rate. Figure 25 depicts the LOTEM field arrangement. Nearly 9 hours of Ex-component time series data were collected over three fracturing stages at a depth of 2800 m, facilitating comparative investigations of each stage.
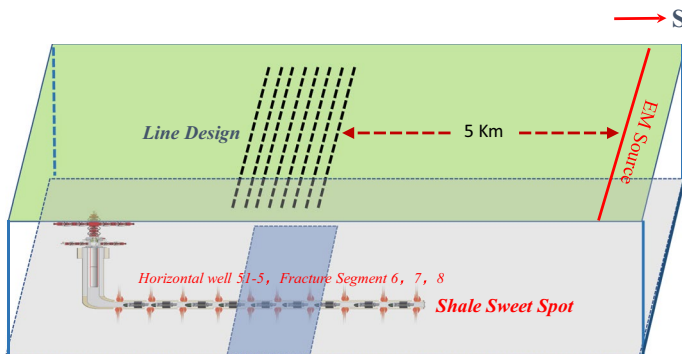

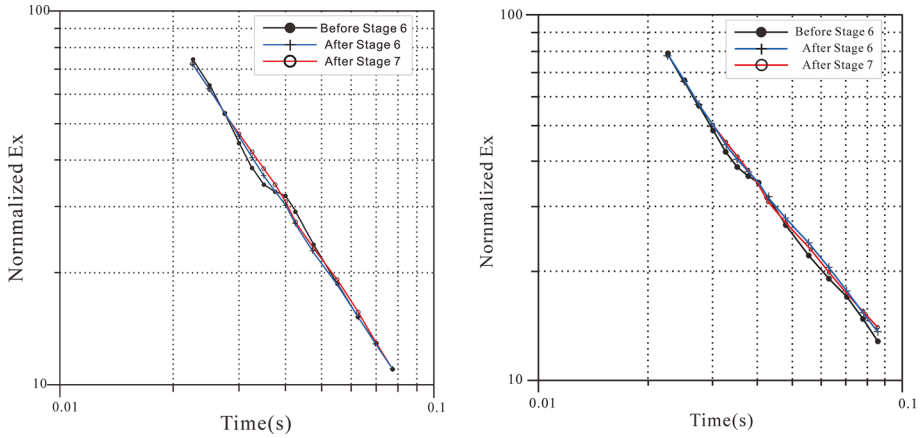**Fig. 25** LOTEM Layout for the monitoring of shale fracture

Fig. 26 The normalized electric field residual curves of site L01-14 (left) and site L01-16 (right) over the stage 6th and 7th (Yan et al. 2018)
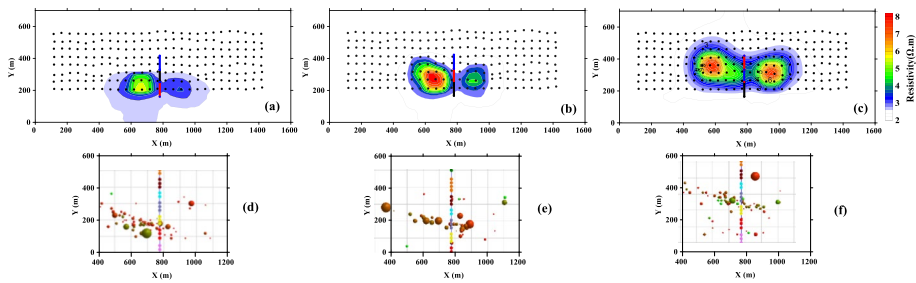

Fig. 27 Fracture fluid anomalies imaged by LOTEM in comparison with micro-seismicity events at after stages 6, 7, and 8, respectively (Yan et al. 2018)

In order to guarantee the stacking effect, the 30-min electric field component time series in stages 6th, 7th, and 8th are extracted for stacking, yielding the normalized electric field residual curve. Fig. 26 exhibits the normalized electric field residual curve of site L01-14 and site L01-16, illustrating the subtle changes caused by fracturing in the decay curves, and the response time window spans from 0.03 to 0.06 s. The "X" shape and time window align with the forward results shown in Fig. 26.

Utilizing NDDR parameters, the electrical anomaly distribution at a depth of 2,340 m in the reservoir stimulation region post-fracturing was derived via the 4D residual imaging methodology, guided and calibrated by well logging and seismic data. Figure 27a–c, respectively, depicts the planar images of fracturing fluid anomalies succeeding the 6th, 7th, and 8th fracturing stages. The progression of fracturing stages reveals a gradual amplification of the anomaly with improved definition. This can be attributed predominantly to the injection of 2,000 m^3 of fluid and proppant into the reservoir at each stage, with each stage separated by an interval of 80 m. Due to the continuous lateral injection during hydraulic fracturing, the fracturing fluid anomaly is horizontally dispersed. Following the 6th stage of fracturing, the fracturing fluid anomaly spans approximately 600 m from east to west (400 m westward from the horizontal well and 200 m eastward). The north-south

breadth measures around 200 m. Post the 8th stage of fracturing, the east-west extent of the fracturing fluid anomaly approximates to 800 m, while the north-south width broadens to 300–400 m. Collectively, the fracturing fluid direction and spatial distribution form a dumbbell shape, with the western volume and height surpassing the eastern ones. This signifies a superior fracturing effect to the west of the horizontal well compared to the east. Figure 27d–f represent the planar distribution of micro-seismic events of the three fracturing stages, monitored concurrently by the micro-seismic method. This reveals that the shape and volume of fracturing fractures are analogous to the anomaly shape and volume monitored by LOTEM. Upon juxtaposing the LOTEM results with micro-seismic, both good agreement and discernible differences emerge. The fracturing fractures' body direction as monitored by micro-seismic is notably NWW, while the fracturing fluid anomaly direction as monitored by LOTEM is nearly EW.

The 4D LOTEM processing and imaging outcomes demonstrate that the electrical alterations stemming from shale reservoir fracturing can be observed at ground level. The spatial fracturing fluid distribution can be determined under the constraints of geological, well logging, and seismic data. The monitoring study results bear significant implications for unconventional HC fracturing production and drilling adjustments.

5 Discussion and Conclusions

5.1 Discussion

Undoubtedly, the induced polarization phenomena inherent within unconventional hydrocarbon reservoirs precipitate a physical escalation in the resistivity of anomalous entities, thereby exerting influence upon the electromagnetic field. The deployment of a methodological framework that judiciously harnesses the information gleaned from induced polarization for the elucidation of sweet spot anomalies within unconventional reservoirs is grounded in scientific cogency. Nevertheless, it is imperative to acknowledge that the electrical anisotropy inherent in unconventional reservoirs similarly culminates in a substantial amplification of vertical resistivity. For instance, shale manifests an anisotropy coefficient surpassing 10, which consequently induces alterations in electrical anomalies in the order of 20% to 30%. The assiduous exploitation of this anisotropic hallmark is instrumental in refining the accuracy of reservoir fluid characterization. It is manifestly evident that an efficacious enhancement in the domain of electromagnetic exploration for unconventional hydrocarbons necessitates a comprehensive consideration of both induced polarization effects and the challenges presented by electrical anisotropy within the reservoir.

Pertaining to the delineation of sweet spots and mechanism of IP effect within unconventional hydrocarbon repositories, there emerges a conundrum concerning the detection modality. Empirical data derived from rock physics experimentation, in conjunction with the pragmatic implementation of CSEM methodologies in hydrocarbon reconnaissance, unveil the propensity of conventional reservoirs to manifest a synthesis of elevated resistivity and pronounced polarization. In contrast, the organic-laden shales indigenous to the southern regions of China are rich in pyrite by an amalgam of attenuated resistivity and heightened polarization, with the latter bearing a linear correlation with the TOC content within the sweet spots and mechanism of IP effect. This distinct attribute holds substantial merit, both theoretically and pragmatically, in the context of shale gas sweet spot delineation. However, it is imperative to recognize the absence of universality in this detection

paradigm, as manifested by the divergent characteristics of tight sandstone and limestone reservoirs. Hence, it becomes imperative to undertake a rigorous and comprehensive analysis of the IP mechanism and the identification of the sweet spot utilizing the CSEM method in the domain of unconventional oil and gas exploration. Herein, rock physics emerges as the cornerstone upon which the research into the electromagnetic characterization of sweet spots is predicated.

Prerequisite to data assimilation, a meticulous tripartite amalgamation of feasibility analyses, construction schematics, and in situ experimentation is indispensable to the procurement of superior datasets. This constituent phase, lamentably, has been met with a dearth of due cognizance within the confines of China and is habitually subjected to a cursory execution. Capitalizing on the comprehensive assemblage of geological, rock physics, electric well logging, and seismic data is imperative for the construction of the geoelectric model encompassing the acquisition domain, with an emphasis on the reservoir's anisotropic model. Engaging in three-dimensional forward simulations, the objective is to discern the responsive attributes of varying electromagnetic field components vis-à-vis the target entity, deploying an array of observational apparatus parameters, culminating in the identification of an optimal observation stratagem. Electric components display sensitivity toward strata with heightened resistivity, while their magnetic counterparts exhibit an affinity for layers of diminished resistivity. Tensor source excitation is propitious for the observation of the reservoir's electrical anisotropy, thereby mandating the employment of tensor source emissions concomitant with a multi-component acquisition modality within the electromagnetic techniques espoused for unconventional hydrocarbon exploration. Albeit, it is noteworthy that the acquisition of magnetic field components is beleaguered by the terrain and electromagnetic perturbations, as exemplified by WFEM's exclusive collection of electric field components, and LOTEM's proclivity for electric field collection within the Chinese experimental precincts. This predicament not only imposes inordinate challenges upon data manipulation and inversion but also engenders an escalation in the non-uniqueness of interpretations due to the paucity of magnetic field components. The acquisition of data via terrestrial CSEM exploration is inherently susceptible to a plethora of external factors, culminating in an attenuation of signal quality. The augmentation of transmitter potency and the escalation of emission currents emerge as germane countermeasures; albeit, they are not without the encumbrance of Safety, Health, and Environmental (SHE) considerations. The intensity of the signal is directly proportional to the source dipole moment (a function of emission current and source pole distance), and assiduously curbing grounding resistance while maintaining moderated voltages emerges as a scientifically robust methodology to optimize supply currents, thereby bolstering the S/N ratio.

From a methodological vantage point, PRBS technology is emblematic of an exceedingly elevated S/N ratio conjoined with an robust imperviousness to perturbations. Its applications bifurcate into two salient dimensions. Primarily, in the realm of frequency-domain controlled source electromagnetics, transmissions are orchestrated utilizing pseudo-random timing signals predicated on 2^n sequences. This paradigm facilitates the simultaneous emission and reception across a multifarious array of frequencies, thus not merely amplifying the S/N ratio, but concomitantly bolstering operational alacrity, as evidenced in the WFEM modality. As an auxiliary application, time-domain controlled sources employ M-sequence pseudo-random timing waveforms for transmission. By engaging in a correlative analysis of the received signal's temporal series with the M-sequence, it becomes feasible to procure the geoelectric impulse response, thus paving the way for the instauration of time-domain data processing, inversion, and interpretational techniques. It is imperative

to underscore that this technique is still in its incipient stages, and the constrained exploration depths warrant an intensified commitment to rigorous research and development.

Within the geophysical community, there has been a sustained interest in the exploration of methodologies for defining apparent parameters in controlled source electromagnetics, predicated upon the half-space model. One archetypal example is the all-zone apparent resistivity, which has demonstrated efficacy in facilitating qualitative data inversion and interpretation. Nevertheless, in light of advancements in inversion techniques, 3D inversion of CSEM often obviates the necessity for apparent resistivity parameters, instead capitalizing on normalized observational field values for inversion purposes. From this vantage point, the endeavor to define electromagnetic attribute parameters may seem to hold limited value. However, the role of electromagnetic attribute parameters in establishing initial models for inversion, as well as in guiding and critically assessing the performance of 3D inversion, cannot be underestimated. This, in turn, can significantly ameliorate the issue of non-uniqueness in inversion outcomes. Consequently, the pursuit of defining all-zone apparent parameters continues to be of practical importance and scientific relevance.

To actualize the discernment of fluid attributes in deep reservoirs and the detection of sweet spots utilizing controlled source electromagnetic methods, mere dependence on the intrinsic multiplicity of source excitations, observational components, and joint inversion parameters is demonstrably inadequate. It is noteworthy that throughout the phase of hydrocarbon exploitation, there exists a plethora of seismic and well-logging datasets. Consequently, elementary attributes encompassing subterranean structural configurations and the spatiotemporal disposition of the targets are well-established. The mandate of the electromagnetic methodology is primarily focused on the determination of reservoir fluid properties, alongside the amplitude and spatial allocation of their characteristic attributes. Under such constraints, the scope of electromagnetic inversion is inherently restricted, and the count of model parameters is comparatively nominal. Integration of well-seismic constraints within the inversion framework is poised to significantly augment both the fidelity and robustness of fluid identification and sweet spot detection endeavors.

5.2 Conclusions

Our understanding of unconventional hydrocarbon reservoirs has been significantly enriched by this study, particularly emphasizing the crucial strides in the experimental research of their electrical properties. The intricate resistivity evaluations indicate that unconventional hydrocarbon rocks in Southern China manifest unique electrical characteristics: low resistivity and heightened induced polarization, an attribute that's reflective of the areas subjected to hydraulic fracturing reservoir stimulation.

Analyzed logging data and shale rock samples substantiate the positive correlation between the TOC content in sweet spots and their resistivity and polarizability. This compelling evidence provides robust petrophysical substantiation for the utilization of CSEM methodologies for unconventional hydrocarbon reservoir exploration and sweet spot detection. Moreover, the deployment of the sweet spot TOC prediction model, derived from the induced polarization parameters of shale samples, has demonstrated remarkable progress, especially in evaluating unconventional hydrocarbon reservoirs. This advancement has elicited substantial attention in the petroleum industry. Simultaneously, the integration and application of novel technological strategies and methodologies have significantly amplified the flexibility of CSEM methods, resulting in marked enhancements in the quality of

data gathered. The tactics, including high spatiotemporal density data collection, high-power transmitters, PRBS, reference observation, and multiscale signal processing, have notably boosted the S/N ratio of CSEM, ensuring the collection of superior quality data conducive to precise inversion.

The initiation of novel EM attribute parameters and a multi-parameter joint identification methodology has augmented the sensitivity and dependability of CSEM in identifying sweet spots and determining fluid properties, thereby aiding in geological interpretation. The creation of sweet spot detection models and parameter prediction methodologies, rooted in the EM characteristics of shale reservoirs, set a robust physical basis for the use of EM methodologies in geological evaluations. Additionally, the 4D CSEM method has been rigorously tested in monitoring hydraulic fracturing in unconventional oil and gas fields within China, delivering encouraging geological results. Despite the primary mode of data interpretation being 4D data processing and imaging, the time-lapse processing and interpretation of 3D inversion are still to fully mature. Nonetheless, the synthesis of these findings offers a comprehensive portrayal of the progression in CSEM methodologies, underscoring their effectiveness and potential in the exploration and assessment of unconventional hydrocarbon reservoirs.

Declarations

Conflict of interest The authors declare no conflict of interest.

References

Adao F, Ritter O, Spangenberg E (2016) The electrical conductivity of Posidonia black shales from magnetotelluric exploration to rock samples. Geophys Prospect 64(2):469–488. https://doi.org/10.1111/1365-2478.12288

Allegar NA, Strack KM, Mittet R, et al (2008) Marine time domain CSEM—the first two years of experience. In: 70th EAGE Conference & Exhibition, Rome, Italy

Astic T, Oldenburg DW (2019) A framework for petrophysically and geologically guided geophysical inversion using a dynamic Gaussian mixture model prior. Geophys J Int 219(3):1989–2012. https://doi.org/10.1093/gji/ggz389

Börner FD, Schopper JR, Weller A (1996) Evaluation of transport and storage properties in the soil and groundwater zone from induced polarization measurements. Geophys Prospect 44:583–601. https://doi.org/10.1111/j.1365-2478.1996.tb00167.x

Burtman V, Zhdanov MS (2015) Induced polarization effect in reservoir rocks and its modelling based on generalized effective-medium theory. Resour-Effic Technol 1(1):34–48. https://doi.org/10.1016/j.reffit.2015.06.008

Burtman V, Zhdanov MS, Fu H (2014) Spectral induced polarization effect in unconventional reservoir rocks. SEG Tech Program Expand Abstr 33:907–911. https://doi.org/10.1190/segam2014-0419.1

Chen B, Li J, Zhou F (1999) Quasi wave equation migration of transient electromagnetic field. Oil Geophys Prospect 34(5):546–554 (**in Chinese**)

Chen F, Xiu J, An J, Liao C, Chen D (2000) Research on dependence of resistivity changing anisotropy on microcracks extending in rock with experiment. Acta Seismol Sin 22(3):331–341. https://doi.org/10.1007/s11589-000-0043-6

Chen L, Wang Y, Zhang C (2021) Anisotropy of complex resistivity of the shale in eastern Guizhou province and its correlations to reservoir parameters of shale gas. Chin J Geophys 64(9):3344–3357. https://doi.org/10.6038/cjg2021O0273. (**in Chinese**)

Commer M, Newman GA, Williams KH, Hubbard SS (2011) 3D induced-polarization data inversion for complex resistivity. Geophysics 76(3):F157–F171. https://doi.org/10.1190/1.3560156

Constable S (2010) Ten years of marine CSEM for hydrocarbon exploration. Geophysics 75(5):75A67-75A81. https://doi.org/10.1190/1.3483451

Davydycheva S, Rykhlinski N, Legeido P (2006) Electrical-prospecting method for hydrocarbon search using the induced-polarization effect. Geophysics 71(4):G179–G189. https://doi.org/10.1190/1.2217367

Davydycheva S, Geldmacher I, Hanstein T, et al (2017) CSEM revisited—shales and reservoir monitoring. In: 79 th EAGE conference and exhibition 2017, pp 12–15. Paris, France (2017)

De Lima OAL, Sharma MM (1992) A generalized Maxwell-Wagner theory for membrane polarization in shaly sands. Geophysics 57(3):431–440. https://doi.org/10.1190/1.1443257

Di Q, Wang M, Wang R, Wang G (2008) Study of the long bipole and large power electromagnetic field. Chin J Geophys 51(6):1917–1928 (**in Chinese**)

Di Q, Lei D, Wan Z et al (2016) An integrated test of the multi-channel transient electromagnetic system. Chin J Geophys 59(12):4399–4407 (**in Chinese**)

Di Q, Zhu R, Xue G, Yin C, Li X (2019) New development of the Electromagnetic (EM) methods for deep exploration. Chin J Geophys 62(6):2128–2138 (**in Chinese**)

Di Q, Xue G, Yin C, Li X (2020) New Methods of controlled-source electromagnetic detection in China. Sci China (earth Sci) 63:1268–1277

Fiandaca G, Auken E, Christiansen AV, Gazoty A (2012) Time-domain-induced polarization: full-decay forward modeling and 1D laterally constrained inversion of Cole–Cole parameters. Geophysics 77(3):E213–E225. https://doi.org/10.1190/geo2011-0217.1

Gallardo LA, Meju MA (2003) Characterization of heterogeneous near-surface materials by joint 2D inversion of dc resistivity and seismic data. Geophys Res Lett 30(13):1658. https://doi.org/10.1029/2003GL017370

Gallardo LA, Meju MA (2004) Joint two-dimensional DC resistivity and seismic travel time version with cross-gradients constraints. J Geophys Res Solid Earth 109:B03311. https://doi.org/10.1029/2003JB002716

Gao J, Zhang H, Fang H, Li N (2017) An efficient joint inversion strategy for 3D seismic travel time and DC resistivity data based on cross-gradient structure constraint. Chin J Geophys 60(9):3628–3641 (**in Chinese**)

Giraud J, Pakyuz-Charrier E, Jessell M, Lindsay M, Martin R, Ogarko V (2017) Uncertainty reduction through geologically conditioned petrophysical constraints in joint inversion. Geophysics 82(6):1D19-1D34. https://doi.org/10.1190/geo2016-0615.1

Haber E, Oldenburg DW (1997) Joint inversion: a structural approach. Inverse Probl 13:63–77. https://doi.org/10.1088/0266-5611/13/1/006

He J (2010) Wide field electromagnetic sounding methods. J Central South Univ (sci Technol) 41(3):1065–1072

He Z (2019) Opportunities, challenges and development directions of electromagnetic exploration today. Comput Tech Geophys Geochem Explor 41(4):433–447 (**in Chinese**)

He Z, Wang X (2007) Geo-electrical anomalous pattern of reservoir and oil/gas detection by electromagnetic survey. Oil Geophys Prospect 42(1):102–106 (**in Chinese**)

He Z, Liu X, Qiu W et al (2005) Mapping reservoir boundary by borehole-surface TFEM: two case studies. Lead Edge 24(9):896–900. https://doi.org/10.1190/1.2056379

He Z, Hu W, Dong W (2010) Petroleum electromagnetic prospecting advances and case studies in China. Surv Geophys 31(2):207–224. https://doi.org/10.1007/s10712-009-9093-z

He Z, Wu D, Wu L (2012) The current situation and developing trend of domestic large power control source electromagnetic instrument. Equip Geophys Prospect 22(6):351–355 (**in Chinese**)

He Z, Hu Z, Gao Y, He L, Meng C, Yang L (2015) Field test of monitoring gas reservoir development using time-lapse continuous electromagnetic profile method. Geophysics 80(2):WA127–WA134. https://doi.org/10.1190/geo2014-0195.1

He Z, Hu Z, Wang Z, Zhao Y, Shen Y, Liu X (2020) Time-frequency electromagnetic (TFEM) technique: step-by-step constraint inversion based on artificial fish swarm algorithm. Oil Geophys Prospect 55(4):898–905 (**in Chinese**)

He Z, Dong W, Zhao G, Hou Y, Shen Y, Liu X (2021) Time-frequency electromagnetic (TFEM) technology: data processing. Oil Geophys Prospect 56(6):1391–1399 (**in Chinese**)

Heincke B, Jegen M, Moorkamp M, Chen J, Hobbs RW (2010) Adaptive coupling strategy for simultaneous joint inversions that use petrophysical information as constraints. In: SEG technical program expanded abstracts, pp 2805–2809. https://doi.org/10.1190/1.3513426

Hoversten GM, Commer M, Haber E, Schwarzbach C (2015) Hydro-frac monitoring using ground time-domain electromagnetics. Geophys Prospect 63(6):1508–1526. https://doi.org/10.1111/1365-2478.12300

Hu Z, Shi Y, Liu Y, Liu X, Sun W, He Z (2020) Nonlinear constrained joint inversion of MT and gravity. Oil Geophys Prospect 55(01):226–232 (**in Chinese**)

Hu W, Shen J, Yan L (2022) Reservoir fluid prediction Theory with CSEM and application. Science Publish House, Beijing

Jegen MD, Hobbs RW, Tarits P, Chave A (2009) Joint inversion of marine magnetotelluric and gravity data incorporating seismic constraints: Preliminary results of sub-basalt imaging off the Faroe Shelf. Earth Planet Sci Lett 282(1–4):47–55. https://doi.org/10.1016/j.epsl.2009.02.018

Ji Y, Li D, Yuan G, Lin J, Du S, Xie L, Wang Y (2016) Noise reduction of time domain electromagnetic data: application of a combined wavelet denoising method. Radio Sci 51(6):680–689. https://doi.org/10.1002/2016RS005985

Jiang Q (2010) Study on the key technology of wide field electromagnetic sounding instrument. PhD thesis, Central South University

Kavian M, Slob EC, Mulder WA (2012) A new empirical complex electrical resistivity model. Geophysics 77(3):E185–E191. https://doi.org/10.1190/geo2011-0315.1

Lelievre PG, Farquharson CG (2013) Gradient and smoothness regularization operators for geophysical inversion on unstructured meshes. Geophys J Int 195(1):330–341. https://doi.org/10.1093/gji/ggt255

Lelievre PG, Farquharson CG, Hurich CA (2012) Joint inversion of seismic travel times and gravity data on unstructured grids with application to mineral exploration. Geophysics 77(1):K1–K15. https://doi.org/10.1190/geo2011-0154.1

Li X, Xue G, Song J, Guo W, Wu J (2005) An optimize method for transient electromagnetic field-wave field conversion. Chin J Geophys 48(5):1185–1190 (**in Chinese**)

Li D, Di Q, Wang M, David N (2015) 'Earth–ionosphere' mode controlled source electromagnetic method. Geophysics 202(3):1848–1858. https://doi.org/10.1093/gji/ggv256

Liu Y, Yin C, Cai J et al (2018) Review on research of electrical anisotropy in electromagnetic prospecting. Chin J Geophys 61(8):3468–3487 (**in Chinese**)

Liu J, Guo T, Wang B, Guo Z (2021) Review of marine electromagnetic methods for hydrocarbon exploration. Geophys Prospect Pet 60(4):527–538 (**in Chinese**)

Liu X, Zhang C, Zhou Y (2015) Exploration of organic rich shales using a time-frequency electromagnetic method. In: GEM Chengdu 2015: international workshop on gravity, electrical and magnetic methods and their applications Chengdu, China. pp 19–22

Mackie R, Meju M, Miorelli F et al (2020) Seismic image-guided 3d inversion of Marine csem and mt data. Interpretation 8(4):1–43. https://doi.org/10.1190/INT-2019-0266.1

Mittet R (2015) Seismic wave propagation concepts applied to the Interpretation of marine controlled-source electromagnetic. Geophysics 80(2):E63–E81. https://doi.org/10.1190/geo2014-0215.1

Mittet, R (2018) Electromagnetic modelling of induced polarization with the fictitious wave domain method. In: SEG technical program expanded abstracts, pp 979–983. https://doi.org/10.1190/segam2018-2994774.1

Oehler DZ, Sternberg BK (1984) Seepage-induced anomalies, "false" anomalies, and implications for electrical prospecting. AAPG Bull 68(9):1121–1145. https://doi.org/10.1306/AD4616E2-16F7-11D7-8645000102C1865D

Ouyang T, Di Q, Xue G, Lei D (2019) Identifying deep ore bodies using the Multi-Channel Transient Electromagnetic Method (MTEM): an example of a lead-zinc-silver mine in Inner Mongolia. Chin J Geophys 62(5):1981–1990 (**in Chinese**)

Passalacqua H, Strack K (2016) Integrated geophysical reservoir monitoring for heavy oil. SPE. SPE-184089-MS.

Passalacqua H, Davydycheva S, Strack K (2018) Feasibility of multi-physics reservoir monitoring for heavy oil.SPE, SPE-193690-MS.

Peng G, Liu Z (2020) An overview of joint electromagnetic-seismic inversion and its future development. Oil Geophys Prospect 55(2):465–474 (**in Chinese**)

Peng G, Xu K, Du R, Liu Z (2018) Reservoir petrophysical parameter estimation with joint inversion of MCSEM and seismic AVA data. Oil Geophys Prospect 53(05):1110–1116 (**in Chinese**)

Piao H (1990) Principle of electromagnetic sounding. Geological Publishing House, Geological Press, Beijing

Rasmussen S, Nyboe NS, Mai S, Juul Larsen J (2017) Extraction and use of noise models from transient electromagnetic data. Geophysics 83(1):E37–E46. https://doi.org/10.1190/geo2017-0299.1

Seigel H, Nabighian M, Parasnis DS, Vozoff K (2007) The early history of the induced polarization method. Lead Edge 26(3):312–321. https://doi.org/10.1190/1.2715054

Stephan A, Strack KM (1991) Simple approach to improve the S/N ratio for TEM data using multiple receivers. Geophysics 56(6):863–869

Stoffa PL, Ziolkowski A (2018) Time evolution of the electric field—Part 1: using the rapid expansion method (REM) with pseudo-spectral evaluation of spatial derivatives. In: SEG technical program expanded abstracts, pp 898–902. https://doi.org/10.1190/segam2018-2995831.1

Strack KM (2013) Future directions of electromagnetic methods for hydrocarbon applications. Surv Geophys 35:157–177. https://doi.org/10.1007/s10712-013-9237-z

Strack KM, Hanstein T, Lebrocq K, Moss DC, Vozoff K, Wolfram PA (1989) Case histories of long-offset transient electromagnetic (LOTEM) in hydrocarbon prospective areas. First Break 7(12):467–477

Strack KM, Allegar N, Ellingsrud S (2008) Marine time domain CSEM: an emerging technology. In: 19th IAGA WG Beijing 2008 annual meeting extended abstract, pp 736–740

Strack KM (1992) Exploration with deep transient electromagnetics, Elsevier, (reprinted 1999), ISBN: 0-444-89541-8

Streich R (2016) Controlled-source electromagnetic approaches for hydrocarbon exploration and monitoring on land. Surv Geophys 37(1):47–80. https://doi.org/10.1007/s10712-015-9336-0

Streich R, Becken M, Matzander U, Ritter O (2011) Strategies for land-based controlled-source electromagnetic surveying in high-noise regions. Lead Edge 30(10):1174–1181. https://doi.org/10.1190/1.3657078

Su Z, Wu X, Hu W, Zeng J, Gong J, Qing Z, Yan L (2005) Application of complex apparent resistivity (CR) method in prediction of oil/gas. Oil Geophys Prospect 40(4):467–471 (**in Chinese**)

Tietze K, Grayver A, Streich R, Ritter O (2014) Developments for Land-based Controlled-source Electromagnetic Surveying. In: 76th EAGE conference and exhibition—workshops. https://doi.org/10.3997/2214-4609.20140561

Veeken PC, Legeydo PJ, Davidenko YA, Kudryavceva EO, Ivanov SA, Chuvaev A (2009) Benefits of the induced polarization geoelectric method to hydrocarbon exploration. Geophysics 74(2):B47–B59. https://doi.org/10.1190/1.3076607

Vinegar HJ, Waxman MH (1984) Induced polarization of shaly sands. Geophysics 49(8):1267–1287. https://doi.org/10.1190/1.1441755

Wang M, Chen C, Qu D et al (2015) The geophysical characteristics of shale gas reservoir from Wufeng member to Longmaxi member in Jiaoshiba block of Fulin shale gas field. Geophys Prospect Pet 54(5):613–620 (**in Chinese**)

Wang X, Di Q, Den J (2016) Multichannel transient electromagnetic method for dynamic detection of oil and gas reservoirs. Pet Geophys Exp 51(5):1021–1030 (**in Chinese**)

Wang X, Li J, Jiang W, Zhang H, Feng Y, Yang Z (2022) Characteristics, current exploration practices, and prospects of continental shale oil in China. Adv Geo-Energy Res 6(6):454–459. https://doi.org/10.46690/ager.2022.06.02

Wu C et al (1996) The application of complex resistivity method in oil field exploration. Geophys Prospect Pet 35(4):111–118

Wu S, Huang Q, Zhao L (2021) De-noising of transient electromagnetic data based on the long short-term memory-autoencoder. Geophys J Int 224(1):669–681. https://doi.org/10.1093/gji/ggaa424

Xiang K, Hu W, Yan L, Zhang C, He W, Tang X, Liu X (2014) Complex resistivity dispersion characteristics of shale samples in Sichuan and Guizhou area. Oil Geophys Prospect 49(5):1013–1019 (**in Chinese**)

Xiang K, Yan L, Hu H, Hu W, Tang X, Liu X (2016) Relationship analysis between brittle index and electrical properties of marine shale in South China. Geophys Prospect Pet 55(6):894–903 (**in Chinese**)

Xiang K, Yan L, Tan G, Luo Y, Yu G (2022) Complex resistivity anisotropy response characteristics of wufeng-longmaxi formation shale in Southern Sichuan. Minerals 12:1395. https://doi.org/10.3390/min1211139

Xu F, Yan L, Xiang K, Tong X, Xie X (2020) Predicting the characteristic parameters of shale sweet-spot with complex resistivity. Terr Atmos Ocean Sci J 31(5):497–505

Xue G, Chen W, Wu X, Guo W, Yue J, Yu J (2020a) Review on research of short-offset transient electromagnetic method. J China Univ Min Technol 49(2):215–226

Xue G, Di Q, Wang R, An Z, Fu C, Li X, Li H (2020b) Overview on data processing methods of multi-channel transient electromagnetic method. Progress Geophys 35(1):0211–0215 (**in Chinese**)

Yan L, Hu W, Chen Q, Hu J (1999) The estimation and fast inversion of All-time apparent resistivity for LOTEM. Oil Geophys Prospect 34(5):532–538 (**in Chinese**)

Yan L, Chen X, Tang H, Xie X, Zhou L, Hu W, Wang Z (2018) Continuous TDEM for monitoring shale hydraulic fracturing. Appl Geophys 15(1):26–34. https://doi.org/10.1007/s11770-018-0661-1

Yan Z, Tan H, Peng M, Kong W, Wu P (2020) Three-dimensional joint inversion of gravity, magnetic and magnetotelluric data based on cross-gradient theory. Chinese J Geophys 63(2):736–752 (**in Chinese**)

Yan L, Xie X, Lou X, Xu Z (2012) Magnetic reference technique and correction method in 3D CSAMT. In: SEG technical program expanded abstracts, pp 1–5. https://doi.org/10.1190/segam2012-0239.1

Yan L, Xiang K, Li P, Liu X, Wang Z (2014) Study on the induced polarization model in the exploration for shale gas in southern China. In: SEG technical program expanded abstracts, pp 912–916. https://doi.org/10.1190/segam2014-0186.1

Yang S (1986) A single apparent resistivity expression for loop-offset transient electromagnetics. Geophysics 51(6):1291–1297. https://doi.org/10.1190/1.1442182

Yang B, Zhang X, Liu Z, Xu K (2021a) Technique and application of joint magnetotelluric and seismic modelling and constrained inversion based on clustering and multivariate geostatistics. Oil Geophys Prospect 56(03):670–677 (**in Chinese**)

Yang Y, He J, Li D (2021b) Energy distribution and effective components analysis of 2 sequence pseudo-random signal. Trans Nonferrous Met Soc China 31(2021):2102–2115

Yuan B, Diquan L, Bayless RC (2017) Wide field electromagnetic method for shale gas exploration in Southern China: a case study. J Environ Eng Geophys 22(3):279–289. https://doi.org/10.2113/JEEG22.3.279

Yuan Z, Zhang Y, Zheng Q (2018) Quantitative evaluation of noise immunity and optimization of coding parameters of M sequences in MTEM method. Oil Geophys Prospect 53(1):195–205 (**in Chinese**)

Zhang C, Liu X, He L, He W, Zhou Y, Zhu Y, Cui Z, Kuang X (2013) A study of exploration organic rich shales using Time-Frequency Electromagnetic Method (TFEM). Chin J Geophys 56(9):3173–3183 (**in Chinese**)

Zhang C, Liu X, Zhou H et al (2015) A step forward study for the exploration of organic-rich shale by using time-frequency electromagnetic method (TFEM). Geophys Prospect Pextroleum 54(5):627–634 (**in Chinese**)

Zhang Q, Li D, Tian M (2017) Application of wide field electromagnetic method to the hydrocarbon exploration in a basin of South Jiangxi. Oil Geophys Prospect 52(5):1085–1092 (**in Chinese**)

Zhao B et al (2006) The PS100 high precision earth-electricity instrument system (IP to IP) with controllable source─application of CDMA technology to the measurement of earth-resistivity for the first time. Progress Geophys 21(2):675–682 (**in Chinese**)

Zhdanov MS, Gribenko AV, Wilson GA, Funk C (2012) 3D joint inversion of geophysical data with Gramian constraints: a case study from the Carrapateena IOCG deposit. South Australia Lead Edge 31(11):1382–1388. https://doi.org/10.1190/tle31111382.1

Zhou C, Tang J, Pang C, Hu S (2019) A theory and simulation study on the space-time array hybrid source electromagnetic method. Chin J Geophys 62(10):3827–3842 (**in Chinese**)

Zhuo X, Zhao G, Di Q, Bi W, Tang J, Wang R (2007) Preliminary application of WEM in geophysical exploration. Progress Geophys 22(6):1921–1924 (**in Chinese**)

Zonge KL, Wynn JC (1975) recent advance and application in complex resistivity measurement. Geophysics 40(5):851–864. https://doi.org/10.1190/1.1440572

Zou C, Zhai G, Zhang G et al (2015a) Formation, distribution, potential and prediction of global conventional and unconventional hydrocarbon resources. Pet Explor Dev 42(1):13–25 (**in Chinese**)

Zou C, Zhu R, Bai B et al (2015b) Significance, geologic characteristics, resource potential and future challenges of tight oil and shale oil. Bull Mineral Petrol Geochem 34(1):3–17 (**in Chinese**)

Authors and Affiliations

Liangjun Yan[1,2,3]

✉ Liangjun Yan
   yljemlab@163.com

1   Key Laboratory of Exploration Technologies for Oil and Gas Resources (Yangtze University), Ministry of Education, Wuhan 430100, China

2   Cooperative Innovation Center of Unconventional Oil and Gas, Wuhan 430100, China

3   Key Laboratory of Geophysical Prospecting, CNPC, Beijing 102249, China